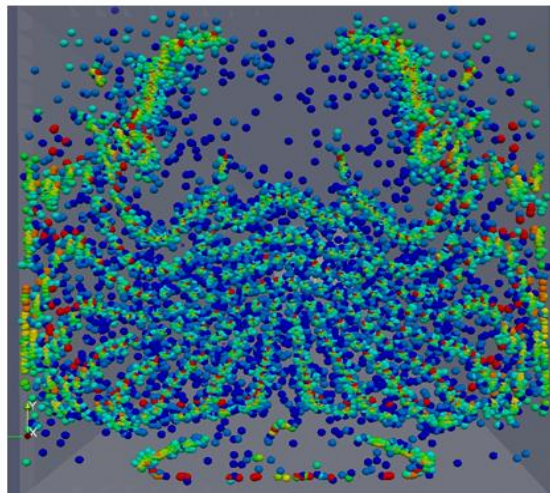


CHALMERS



Design of an optimal oxidation catalyst for particle trapping

Master of Science Thesis



Rodrik Fällmar

Department of Chemical and Biological Engineering

Division of Chemical Reaction Engineering

CHALMERS UNIVERSITY OF TECHNOLOGY

Göteborg, Sweden, 2010

Design of an optimal oxidation catalyst for particle trapping

Rodrik Fällmar

Examiner:

Professor Bengt Andersson, Chemical Reaction Engineering, Chalmers University of
Technology

Supervisor:

Phd student Henrik Ström

Master of Science Thesis

Department of Chemical and biological engineering

Division of Chemical Reaction Engineering

CHALMERS UNIVERSITY OF TECHNOLOGY

Göteborg, Sweden 2010

Design of an optimal diesel oxidation catalyst for particle trapping

Rodrik Fällmar

© RODRIK FÄLLMAR 2010-04-09

Department of Chemical and Biological Engineering

Division of Chemical Reaction Engineering

Chalmers University of Technology

412 96 Göteborg, Sweden

Phone + 46 (0)31-772 1000

Cover: Outlet of a monolith flow through catalyst covered with particles.

Abstract

Diesel engines emit complex mixtures of inorganic and organic compounds in the form of both solid and vapour phase particles. Most of the total numbers of particulates released are ultrafine nanoparticles which are detrimental to human health and can easily enter the body by respiration. The emissions standards on particulate matter release from diesel engines are constantly upgraded within the European Union and with future regulations based on the particles numbers released instead of merely mass, the need for effective aftertreatment devices will increase. Today standard particulate filters in the form of wall flow filters can have problems with high soot accumulation, producing a large exhaust backpressure. A potential solution would be to combine the standard filter with a flow through filter to reduce the load on the wall flow filter.

In this study soot particle trapping has been simulated in different continuous flow filters of monolithic structure including the use of promoters, at laminar flow conditions. An Euler Lagrange model, the discrete phase model in Fluent was used with user defined functions for forces acting on particles. A method to quickly screen trapping of 5 nm and 10 nm particles in different catalysts designs with tracers was also developed. Simulations of square duct monoliths with promoters show that the strength of the vortices produced are not enough to give a high amount of particle deposition on the catalyst walls. The smallest particles in the simulations, 5 and 10 nm particles were trapped to a higher extent, than larger particles up to 1000 nm, in all studied geometries with the predominant deposition mechanism being Brownian diffusion. The comparison of the different filters designed with a wall flow filter does show that the options for altering a design of a flow through filter, without imposing a too large pressure drop penalty are good.

Keywords: Diesel particulate matter, flow through filters, Euler Lagrange, discrete phase model, Fluent.

Preface

This master thesis was performed at the department of Chemical Engineering at Chalmers University of technology. The purpose was to improve the understanding of how particle trapping in continuous flow monolith catalysts could be optimized while still considering pressure drops and other parameters.

I would like to thank my supervisor PhD student Henrik Ström for all the help and time given. The Euler Lagrange simulations in Fluent were sometimes computationally demanding with simulation times ranging up to a week on an ordinary desktop computer. Henrik instructed me on the use of parallel computing, journal and script files and also had the time to set up server simulations, for shorter simulation times. And always had time to discuss and explain things when asked, for that I'm very grateful.

Additionally I would like to thank, Professor Bengt Andersson for his advice and discussions regarding catalyst design. Whenever the master thesis seemed to be at a standstill he gave valuable suggestions on where to continue and encouraged me to learn the new Ansys workbench. Regarding the Ansys workbench and the design modeler tool, I received a lot of help from PhD student Per Abrahamson who deserves great thanks.

In the end the workbench unfortunately did not become as important a tool for this thesis as expected. The demand for specific meshing options, easier achieved in Gambit and Fluent, like meshing certain areas, faces, boundary conditions, size functions among other things somewhat limited the use of it. However learning the latest software is always interesting and valuable for my upcoming future career. Additionally I would like to thank all others who supported me and the people within Competence Center for Catalysis who invited me to Christmas dinner, an enjoyable occasion.

Table of contents

1	Introduction	2
1.1	Background	2
1.2	Objectives.....	3
1.3	Methods.....	3
1.4	Limitations	3
2	Theory	4
2.1	Diesel particulate matter.....	4
2.1.1	Diesel PM Emission	4
2.1.2	Diesel particle size distribution and composition	4
2.2	Aftertreatment technologies	6
2.2.1	Diesel Oxidation catalysts	7
2.2.2	Diesel particulate filters	8
2.2.3	Modification of monolithic flow through filters	8
2.2.4	Pressure drop in monolithic catalysts.....	11
2.2.5	Characterization of Diesel Exhaust flows	12
2.3	Computational fluid dynamics	13
2.3.1	Fundamental equations.....	13
2.3.2	Euler Lagrange particle tracking	14
2.3.3	Lagrangian point particle approach.....	15
2.3.4	Modelling of forces acting on soot particles and deposition mechanisms.....	16
3	Methods.....	18
3.1	Simulation methods.....	18
3.2	The Discrete phase model and UDF:s.....	18
3.2.1	Drag.....	18
3.2.2	Time step.....	19
3.2.3	Body forces	19
3.2.4	Injection Routine	20
3.3	The Species method	20
3.4	General conditions and boundary conditions	21
3.5	Simulation of forces acting on a particle in a vortex.....	22
3.6	Geometry 1: monolith channel with promoter	22
3.7	Geometry 2: monolith channel with four promoters	23
3.8	Geometry 3: monolith channel with planes.....	24
3.9	Geometry 4: monolith channel with tortuous path.....	25
3.10	Geometry 5: Porous promoter	25

3.11 Mesh	26
3.12 Convergence Criteria.....	27
4 Results	28
4.1 Particle movement in a Vortex	28
4.2 Results for Geometry one.....	28
4.3 Results for Geometry two	32
4.3.1 Transient simulation case 2.1	33
4.3.2 Flow velocity effects	34
4.4 Results for Geometry 3	35
4.5 Results for Geometry 4	35
4.6 Results for Geometry 5	36
4.7 Optimum cases all geometries.....	37
4.8 Mass and heat transfer effects	38
5 Conclusions	39
5.1 Further work	40
References	41
Appendix	43

1 Introduction

1.1 Background

The diesel engine is a highly efficient engine which offers good fuel economy. Compared to the gasoline engine it is more efficient with lower fuel consumption and emissions of CO and HC. The major drawback is the release of particulate matter and NO_x which is not a problem in gasoline engines due to effective three-way conversion (TWC) catalysts.

In the diesel engine combustion process there is an excess of air present and thereby oxygen, producing an environment where the TWC cannot be used for reduction of NO_x. Therefore different aftertreatment solutions must be applied: the diesel oxidation catalyst can oxidize HC, CO, NO_x and volatile organic compounds. While there are several options available for reduction of NO_x, one is selective catalytic reduction (SCR).

Diesel engine emissions consist of a complex mixture of organic and inorganic compounds in both solid phase particles and vapour phase. Over 90 % of the total number of particulates released has a diameter of < 1 μm and can easily enter the body by respiration. These particles can have hundreds of chemicals adsorbed on their surfaces among them mutagens and carcinogens [1]. The specific health effect of diesel particulate matter is difficult to study since it is only one source of air pollutant among many but include cancer and cardiovascular diseases. In Europe alone it is estimated that over hundred thousand peoples die prematurely every year because of anthropogenic particulate matter [2].

The regulations on particulate matter release from diesel engines are constantly upgraded within the European Union. With upcoming stricter emission standards in the future such as Euro VI, the need for efficient aftertreatment devices in the form of oxidation catalysts and particle filters will increase.

The most effective diesel particulate filters today are wall flow filters where the exhaust gas flow through porous walls and the pore size allows some particles to be filtered in the walls. With time soot particles also accumulates on the walls with a corresponding build up of a filter cake. However problem occurs if the soot loading becomes too high resulting in a large exhaust gas backpressure which in turn increases fuel consumption and deteriorates engine performance. Cleaning of the filter requires a regeneration process to oxidize trapped particulate matter, a process which is still poorly understood and poses a significant technical challenge [3].

To further increase fuel efficiency and the robustness of the aftertreatment systems, it might be beneficial to combine the existing wall-flow filters with flow-through filters. The flow through filter has a lower particle trapping efficiency than the wall flow filters but also benefits from reduced pressure drop. Nevertheless the continuous flow filter could reduce the load on the wall flow filter and the need for regeneration [4]. Depending on the filter design it could be optimized to selectively trap particles of different diameters.

Gasoline application and other fuels might also be in need of particulate filters especially with the introduction of particle number based emission standards. Designing and optimizing particulate filters and oxidation catalysts requires knowledge on particle deposition mechanisms and forces acting on soot particles. Computational fluid dynamics can be a valuable tool in the design and optimization of automotive particulate filters and oxidation catalysts to meet future emission standards while still maintaining fuel economy and engine

performance. The results of reliable simulations are often shorter design time and reduced development cost for exhaust systems. Additional to predictions of the dynamics of the flow, important parameters such as filter efficiency, thermal properties, catalytic regeneration, flow properties and pressure drop can be predicted.

1.2 Objectives

The main objective was to optimize particle trapping efficiency for an oxidation catalyst more specifically a square duct monolith channel by altering the geometric shape and through the use of promoters in the channel. An important design parameter to consider was the resulting pressure drop in the channel which should be kept as low as possible. Otherwise the engine performance might deteriorate and fuel consumption increase. The main objectives can be summarized as follows:

- Suggest a novel design for an oxidation catalyst that is optimized with respect to particle trapping efficiency
- Assess the possibilities to design such a catalyst in a way which is also beneficial from a heat and mass transfer perspective

1.3 Methods

A literature study was made about catalysts and what benefits geometrical design shapes and promoters had on mass and heat transfer characteristics as well soot particle trapping efficiency and pressure drop. This was to gain insight into design options to simulate with computational fluid dynamics simulations for further knowledge on particle trapping. Further the characteristics of exhaust gas from diesel engines and forces acting on soot particles had to be studied in depth.

The simulations were performed on 3D geometries with meshes mostly generated in Gambit. Symmetry options were only possible for one design and 2 D geometries were not considered since often the meshing demand in specific areas would be equally time consuming to perform as for a 3D model. The software used was ANSYS Fluent 12.0 including the new workbench with the design modeler.

1.4 Limitations

Only flow through square duct filters were studied not porous wall flow filters or combinations of both with hole structures interlinking several channels. The later would require periodic boundary conditions and be more difficult and time demanding to simulate. The pressure drop and particle trapping in a porous promoter was also simulated but the soot accumulation not accounted for. The particle forces considered were the most significant for particle deposition, including Brownian force and drag force while for the thermodynamics of the system only isothermal conditions were assumed. The flow conditions gave Reynolds number around 400 for an average flow velocity of 10 m/s so only a viscous laminar model was applied, no turbulence models. Large eddy simulations was an option but not considered since design and method development took precedence. Particles were injected in an equal number all over the inlet with different injection points and distances between the particles. In reality the laminar velocity profile gives a larger number of particles in the core flow and not an equal spreading over the inlet.

2 Theory

2.1 Diesel particulate matter

The following section describes the difficulties in defining and measuring particulate matter, the current and proposed future emission legislation and the composition and size distribution of particulate matter.

2.1.1 Diesel PM Emission

Particulate matter is a broad definition based on the sampling procedure and the chemical species present is not well defined. Diesel particulate matter is measured by sampling gas from the exhaust system, diluting it with air and filtering diluted diesel exhaust at temperatures lower than 52°C. The dilution is performed to give conditions similar to when the exhaust is released from vehicles to the atmosphere. The filtering will capture both solid particles and condensing liquid droplets provided by the dilution. Hence the definition of PM covers both solid and liquid material [8].

The current PM emissions standards are mass based, corresponding to the amount of mass left in the filter after the sampling procedure. Even though studies have shown that ultrafine particles (< 100 nm in diameter) and nanosized particles (< 50 nm in diameter) are detrimental to human health because of their capability to enter the body by respiration and penetrate cell membranes [8].

Defining new emission standards based on the number of particles released is difficult since the number of particles is altered by nucleation and coagulation processes and not conserved like particle mass. Determination of particle sizes and numbers is also more sensitive to the measuring techniques and parameters applied. Regulations based on a normalized number concentration would not only affect diesel engines but also gasoline spark ignition engines [7].

Stricter particle emission regulations and increased knowledge of the effect on human health, has brought emission control strategies, engine design and aftertreatment systems to focus more on reducing the finest fraction of diesel particles and on the number of particles released [7]. Complementary to the mass-based limits, number-based PM limits will be introduced in upcoming legislation standards. The main reason for this is to prevent development of future filters that meet the PM mass limit but still release a high number of ultrafine particles [8].

2.1.2 Diesel particle size distribution and composition

Direct-ignition diesel engines are more energy efficient than spark ignition gasoline engines. However diesel exhaust contains high concentrations of solid particles and relatively large hydrocarbon molecules which tend to adsorb onto the solid particles [5]. Adsorption of hydrocarbons on solid particles is a problem both in sampling of exhaust emissions and as it passes through catalysts.

In diesel particulate concentration measurements, the particle mass collected by a filter will depend highly upon the amount of adsorbed hydrocarbons present. Hydrocarbons remaining adsorbed when passing through a catalyst are not available to the catalyst unless the particle is directly deposited on the catalytic walls. Therefore knowledge on adsorption of hydrocarbons and their composition in exhaust gases is needed [5].

Diesel exhaust mostly contains hydrocarbons of C₁₅ but also a significant amount which is

larger than C_{25} [5]. The diffusivities of these larger molecular compounds are slow and results in poor mass transfer to the surfaces within a catalytic device. About 80 % by mass of the particulate emission consist of solid carbon particles and sulfur compounds [6]. This is also the fraction which is most difficult to oxidize with catalysts at normal diesel exhaust temperatures, 100-500 °C. The remaining amount is mostly adsorbed or condensed hydrocarbons produced from incomplete combustion of diesel fuel and lubricating oils.

The solid part of diesel particulate matter, carbon particles (soot), hydrocarbons and sulfates is formed early in the combustion process and is relatively stable. Soot is formed due to air deficiency caused by incomplete mixing and soot emissions are strongly increased if the air-fuel mixture is enriched to near stoichiometry [7].

Size distributions can be presented based on either a particle mass or particle number distribution. The solid carbon particles are spherical with diameters in the range of 0.01 to 0.08 μm and often combine to form agglomerates with aerodynamic diameters between 0.1 to 1 μm . Airborne particles are irregular and their aerodynamic behaviour is expressed in terms of an ideal spherical particle known as aerodynamic diameter.

Particulate matter is classified into three major size distribution modes, nuclei-, accumulation- and coarse mode. The accumulation mode consists of agglomerates of carbon particles and condensed heavy hydrocarbons and sulfur compounds. The majority of the mass based particulate matter emissions is from the accumulation mode but it constitute very few of the total number of particles.

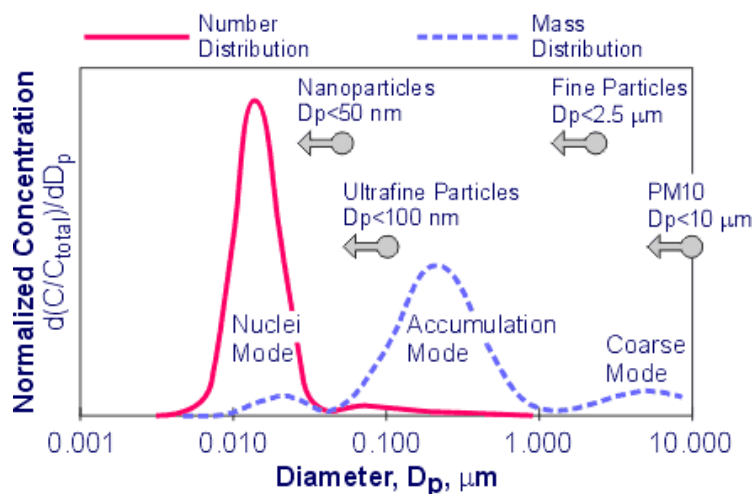


Figure 7: Diesel Particulate Size distribution [8].

At high temperatures most of the hydrocarbons are present in vapour-phase but during cooling in the exhaust pipe, increased adsorption onto carbon particles and condensation processes occurs with formation of nucleated droplets. The nuclei mode particles (carbon particles and nucleated hydrocarbon droplets) is centered near 0.01 μm and usually accounts for only a small fraction of the overall mass but up to 90% of the total number of particles [7].

The coarse mode is comprised of particles not combusted in the diesel engine, for instance particles reentrained from surfaces within the engine and exhaust system. This fraction account for only a small amount of the total PM mass and make almost no contribution to the particle numbers [8].

2.1.3 Emission legislation

In the European Union all diesel vehicles are subject to emission regulations, the test procedures, measurement units and emission standards depend on the vehicle class. One common distinction is made between light and heavy duty vehicles. Heavy-duty vehicles are primarily diesels therefore the diesel emission standards have been set to grams per brake-horsepower-hour or g/kwh. The emissions are normalized according to the total energy output of an engine over the specified driving cycle [9].

The European emission regulations, Euro IV-VI in table 1 apply for new heavy-duty diesel engines of compression ignition type, positive ignition natural gas and LPG engines.

Tier	Date	TEST	CO	HC	NO _x	PM	Smoke
Euro IV	2005.10	ESC & ELR	1.5	0.46	3.5	0.02	0.5
Euro V	2008.10		1.5	0.46	2.0	0.02	0.5
Euro VI*	2013.01		1.5	0.13	0.4	0.01	
*Proposal (2008-12-16)							

Table 1: Eu Emission standards for heavy duty diesel engines, g/kwh (smoke in m⁻¹) [9].

Stricter emission standards for heavy duty engines imposed before 1994 on total particulates and NO_x were reached by engine redesign [7]. When it comes to engine design there is an inverse relation between NO_x and particulates. A rapid complete combustion decreases the particle emissions but on the other hand promotes NO_x formation. The opposite, exhaust gas recycling (EGR), a procedure to lower NO_x emissions instead generally increases particulate emissions [10].

Since NO_x and particulate emissions are difficult to reduce by redesign of diesel engines, fuel changes has also occurred from 1994. Reduction of the sulfur content in fuels, contributes to lower sulfate particulate emissions while decreased content of polycyclic aromatics hydrocarbons decreases the formation of organic carbon particles.

Some other important parameters regulated are cetane number, density and viscosity of the fuels. The cetane number is a measure of combustibility of the fuel and ignition quality of a fuel, the higher the cetane number the smaller the amount of emissions, especially NO_x emissions. Density is an indication of the energy content per unit volume of a fuel where the energy content increases with the density.

The coming Euro VI emission standards will be met by diesel engine manufactures through different exhaust aftertreatment devices, most probably by particulate traps and NO_x reduction catalysts which are only effective at low sulfur levels [10].

2.2 Aftertreatment technologies

The most common type of measure to reduce diesel particulate matter and clean exhaust gas for automotive applications are different filters and oxidation catalysts often of monolith structure. The possibility to modify filters and use promoters for increased particle trapping, heat and mass transfer properties will be described here. The drawback with a modification is usually an increased pressure drop. The equations for pressure drop determination and physical parameters for characterisation of exhaust gas characterisation also have to be considered.

2.2.1 Diesel Oxidation catalysts

The diesel oxidation catalyst (DOC) is designed to oxidize exhaust gases in the presence of oxygen. The most common pollutants oxidized are carbon monoxide (CO), hydrocarbons (HC) and volatile organic compounds in the form of soluble organic fraction (SOF). Nitrogen oxide (NO) is also oxidized to nitrogen dioxide (NO₂) at temperatures of 270°C to 470°C [11], an important reaction which can be undesirable since nitrogen dioxide is more toxic than nitrogen monoxide in nature.

However incineration of solid carbon particles (soot) mostly requires temperatures above 600°C, temperatures diesel exhaust gases cannot reach during normal engine operation. Therefore a diesel particulate filter is often placed downstream from the DOC which utilizes NO₂ to oxidize soot and accumulated particle matters (PM) at temperatures below 350°C [12]. Nitrogen dioxide also enhances regeneration of the filter and the performance for SCR catalysts. Since the temperature of diesel exhaust is low, only a small amount of NO is oxidized to NO₂. The oxidation is further improved if the oxidation catalyst is placed closely to the engine or upstream from the turbocharger [13].

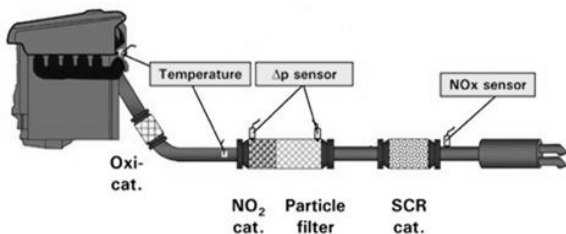
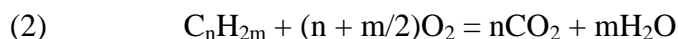


Figure 1: Schematic view of a diesel engine aftertreatment system, the oxidation catalyst is a DOC.

The DOC is usually a honeycomb monolith structure coated with an active catalytic material, a wash coat of precious metals which effectively reduces CO and hydrocarbons emissions through oxidation. One of the most basic washcoat formulations is platinum on alumina (Pt/Al₂O₃) [12]. The effectiveness of the DOC is mostly dependent on the temperature. Below the light off temperature 250°C for a common DOC of Palladium–Rhodium [11], the surface reaction kinetics of the primary chemical reactions determines the performance. Above the light off temperature diffusion of chemical species from the exhaust gases to the solid surface determines the effect of the catalyst that is mass transfer resistances controls the reaction.

The main reactions on the catalytic surface of the DOC are described by reaction 1-3 below where 1 represents the reactions of hydrocarbons to water vapour and carbon dioxide and 2 the oxidation of SOF compounds. Reaction 3 represents the oxidation of carbon monoxide to carbon dioxide [13].



The oxidation reactions in the DOC produce some undesirable products, if sulphur dioxide is oxidized to sulphur trioxide and further reacts with water vapour, sulphuric acid is formed. In the tailpipe or in air, gaseous sulphuric acid adsorbs onto carbon particles and sulphur particles are formed and emitted from the engine.

2.2.2 Diesel particulate filters

The most common type of automotive filter used for particle trapping is the wall flow filter, a catalyst where some of the channels are blocked forcing the flow through porous walls into other channels. Wall flow filters made from ceramic or metallic substrates have a high efficiency, more than 90% of the particulates in the size range of 15 to 500 nm can be captured [14]. A large number of such filters are already installed on mass produced vehicles. The main challenge with such catalysts is not the particle trapping efficiency but the regeneration of the filter system.

Oil and fuel additives can generate ash that clogs the filters and with an increasing amount of soot deposited in the filter, produced from combustion, the backpressure in the engine increases. The regeneration process where soot is incinerated give rise to high temperature peaks which can also mechanically damage the filters, therefore the choice of material for the filter is very important. Silicon carbide and ceramic cordierite are among the most commonly used support materials due to good thermal stability and mechanical strength.

Specialized diesel oxidation catalysts called flow through filters, have open passages for exhaust flow and are made of metallic or ceramic substrates to capture soot. The soot is later oxidized to gaseous products due to reactions with nitrogen dioxide generated in an upstream NO₂ catalyst through regeneration [13]. Tests in non blocking continuous flow catalysts have given particle trapping efficiencies ranging from 20-50% based on different operating conditions [15]. One of the major advantages with the continuous flow filter is the tendency to avoid clogging, in case of insufficient regeneration particles will merely flow through the device [16].

2.2.3 Modification of monolithic flow through filters

A common type of automotive catalyst for exhaust gas cleaning is the monolith catalyst which provides advantages in the form of a large solid-gas interfacial area and low pressure drop. The monolith is usually of a metallic or ceramic material and it is coated with a thin layer of an active catalytic material, a wash coat. Production of monoliths by extrusion of a ceramic material is cheaper than the alternative corrugation technique needed for a metallic alloy. However the later technique is currently becoming more common since it is possible to alter design easier than for a ceramic material [17]. The ceramic monolith is usually found in the square duct form while metallic monoliths are of sinusoidal shape (see figure 2B). Metallic catalysts should be placed near the engine to make use of the lower thermal mass.

The exhaust gas flow encountered in an automotive exhaust system is mostly turbulent upstream from a catalyst. However in the narrow monolith channels a fully developed laminar flow prevails with Reynolds number in the range of 75-600 [18]. At such conditions there is a large resistance to mass and heat transfer in the direction to and from the catalyst wall.

To improve the mass and heat transfer properties, turbulence can be created by introducing obstacles in the metallic monolith channels during the manufacturing process. This concept of introducing promoters has been used both for laminar and turbulent flows successfully for a wide range of applications. Some examples are: heat exchangers, gas cooled nuclear reactors, gas turbine blade cooling, electrochemical reactors and electronic devices [17]. The promoters can be in the form of cylindrical wirers, baffles, wings, corrugated- or sinusoidal channels and improve heat and mass transfer by several hundred percent.

Promoters disturb boundary layers, create swirls and vortices and or intensify generated turbulence. In fully turbulent flows they are mostly placed near the wall to disturb boundary layers. Promoters often reduce the critical Reynolds number which describes the transition from laminar to turbulent flow, from 2300 for a straight duct to 1000-1200 [17]. Already at low Reynolds number a flow disturbance can be observed.

However using promoters reduces the channel area available for flow with the exception for sinusoidal channel configurations which usually do not involve area reduction. Mass and heat transfer rate increases with the improved mass flow rate given by a decrease in channel area. The main disadvantage is an increased pressure drop and in the case of an automotive catalyst, possibly increased fuel consumption.

Andersson and Schön [18] performed CFD simulations on CO and pressure drop in a sinusoidal monolith channel with two promoters shaped as in figure 1. They found that the conversion of CO could be improved by 50% but at the cost of an extensive increase in pressure drop (432%). Another catalyst called Emitec, available commercially, consist of triangular monolith channels of metal with small rounded corrugations, see figure 1. It has been reported to improve mass transfer rates by 15% with a corresponding pressure drop of 14-18% [17].

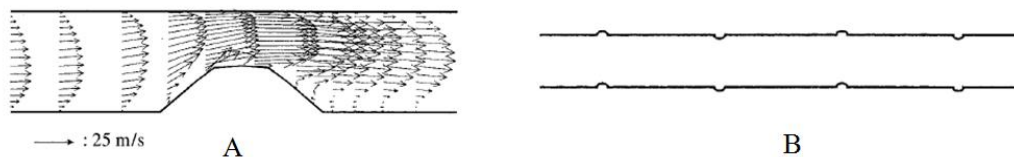


Figure 1: A: sinusoidal monolith channel, B: The Emitec TS catalyst with promoters [11].

Holmgren [17] experimentally measured mass transfer rates and pressure drop in metallic triangular monolith channels (see figure 2) with small protuberances on the wall and compared it to empty straight channels. The introduced promoters did not produce turbulence in large extent but rather disturbed the boundary layers and generated vortices distributing the flows towards the walls. The disturbances was caused by entry effects and the surface roughness of the washcoat and occurred already at low Reynolds numbers which made Holmgren question the accuracy of assuming laminar flows. It was found also found that the increase in mass transfer was larger than the increased pressure drop.

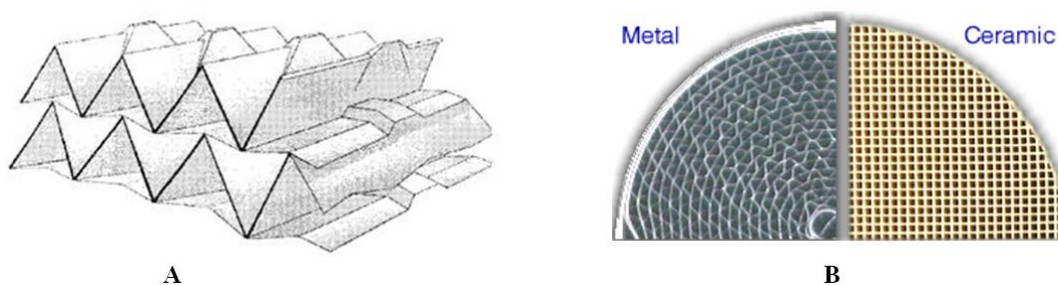


Figure 2: A: Triangular monolith channels with promoters, B: picture of metallic and ceramic monolith.

Particle filters consisting of sinusoidal shaped monoliths channels are found in different forms. These can be either defined as flow through filters or wall flow filters, in figure 3B a typical wall flow filter is shown. Sinusoidal flow through catalysts with open hole structures (see figure 3A) can trap particles in the exhaust gas passing the protrusions. Flow through

filters can also have porous walls giving a filter pressure drop that is lower than for standard wall flow filter [16].

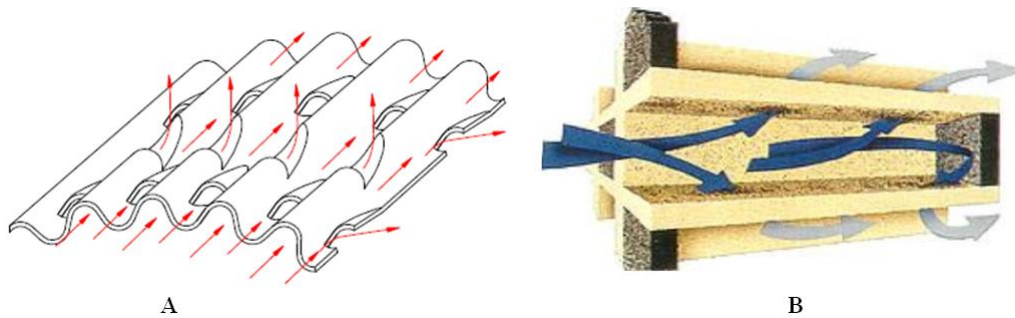


Figure 3: A: sinus wave shaped monolithic metal honeycomb substrate, B: A wall flow monolith [6].

Various kinds of turbulent substrates were developed in 1994 by Emitec [19,20]. One called the transversal structure (see figure 4) consists of small corrugations in the metal substrate, transverse to the flow direction. The corrugations produce radial flow which increases the flow to the walls and thereby the catalytic conversion efficiency. It is also claimed that the lower cell density reduces the backpressure compared to a standard substrate [19].

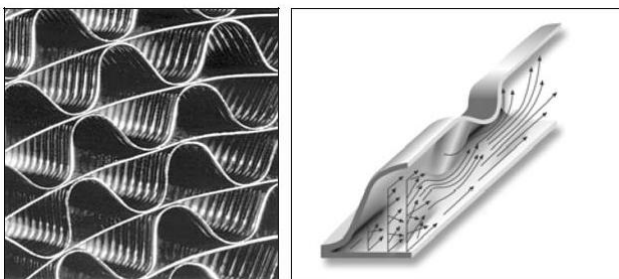


Figure 4: Transversal structure developed by Emitec.

Another structure is the longitudinal foil structure (figure 5) where there are additional cuts and depressions, the channel is broken up by a counter corrugation in the axial direction. This alternative is better than the transversal structure, giving improved mass transfer coefficients and a higher conversion efficiency. Additional benefits are a lower thermal mass which results in lower thermal stress and better use of precious metal which reduce the production cost.

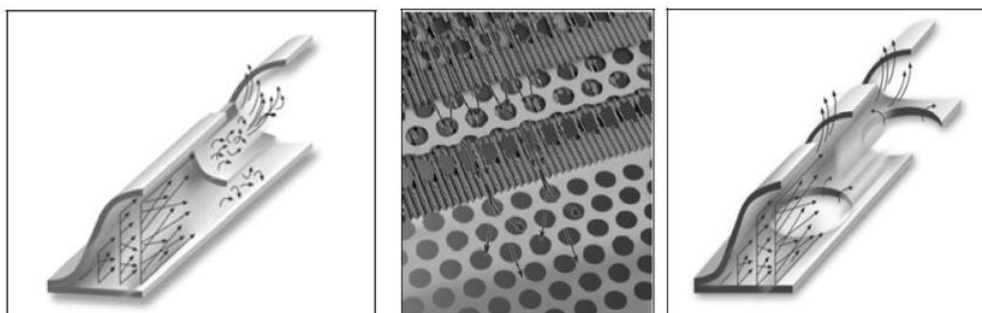


Figure 5: To the left: Longitudinal structure, Right: Perforated structure.

Improved mixing of the exhaust gases in the substrate channels is achieved by introducing holes in the channels [21]. Radial flow through the cavities increases the turbulent mixing and at the same time reduces the backpressure. The structure formed is called a perforated

structure, (figure 5 right) and yields a homogenous distribution of exhaust gas flow and reduced thermal mass [21]. There are also combinations of the longitudinal and perforated structures.

Aniolek [22] performed a two dimensional laminar CFD study on monolithic channels exposed to typical diesel engine exhaust conditions. The channels contained protuberances in the form of round- and rectangular bumps, divots and tortuous paths (seen in figure 6), which are common for metal substrates. A steady state analysis was performed to gain insights on wall protuberances effects on velocity and pressure field, as well as momentum and thermal characteristics [22].

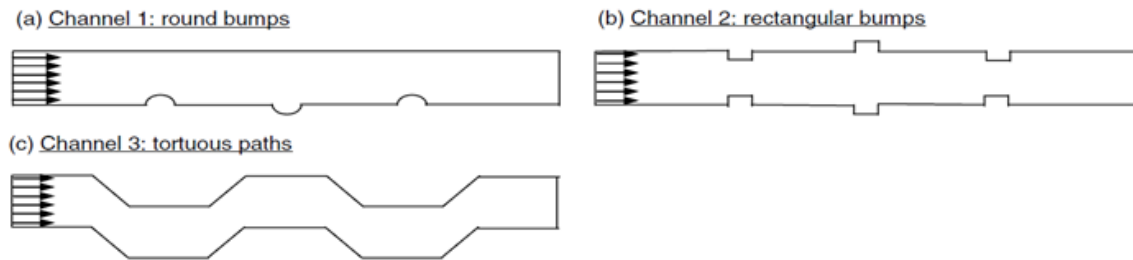


Figure 6: 2D monolith channels with protuberances [22].

An additional transient simulation indicated that a valid steady state solution existed for the three geometries investigated and no shedding or transport of vortices transpired behind the bumps. Steady state recirculation zones are found after every protuberance with low levels of recirculation for the flow. The bumps did not provide any significant flow restriction or effect on the core flow, the adverse pressure gradient and vortices formed downstream of the obstacles is therefore small. The bumps increased the flow velocity while divots, observed in channel 2, figure 6 had small or no effect on flow [22].

The pressure drop increase compared to a straight channel was approximately 25% for squared or round bumps and a factor six for the tortuous path. Channel 3 with the tortuous path design had the highest reversed flow and gave the only increased heat and momentum transport effect. The pressure drops for all three designs will however more than well offset any gain in momentum and heat transport which makes the catalysts unattractive for commercial use. It should be mentioned though that different versions of the three channels already exists as commercial catalysts [22].

2.2.4 Pressure drop in monolithic catalysts

A high backpressure reduces the engine performance and has to be kept at reasonable levels [23]. Automotive catalysts in the form of honeycomb monoliths, consists of several narrow channels with at diameter of roughly 1 mm. The Reynolds number of the flow in a typical catalytic exhaust system is less than $Re_{crit} = 2300$ meaning that a laminar flow prevails in the channels. The pressure drop can then be obtained from the Hagen Poiseuille equation:

$$\Delta P = \frac{A \cdot \mu \cdot v \cdot L}{d_h^2} \quad (2.1)$$

A is a constant depending on the geometrical shape of the channel and d_h is the hydraulic diameter. Additionally inlet and outlet effects occurs which contributes to the overall pressure drop. In the inlet this is due to acceleration of the flow which gives flow separation and in the outlet deceleration transpires. The resulting pressure difference caused by such effects can be estimated with:

$$\Delta P = \frac{1}{2} \rho v^2 \quad (2.2)$$

Representing the kinetic energy of the incoming flow. Furthermore turbulent slugs with small turbulent eddies can appear in the channel at Reynolds numbers of 200-2000 [23]. This is due to that an engine cylinder produces pulsations but the effect is less significant for turbocharged engines with several cylinders. Energy is then lost to the walls giving an increased pressure drop, for prediction of such effects DNS has to be used.

The total pressure drop in the channel can be summed up to:

$$\Delta P = \frac{A \cdot \mu \cdot v \cdot L}{d_h^2} + \frac{B}{2} \rho v^2 \quad (2.3)$$

Andersson and Ekström [10] derived the following expression from experimental studies,

$$\Delta P = \frac{28.4 \cdot \mu \cdot v \cdot L}{d_h^2} + \frac{0.41}{2} \rho v^2 \quad (2.4)$$

Here A=28.4 for a square channel and B is a regression constant. This expression is valid for a non coated monolithic substrate. The Hydraulic diameter, d_h for a square is simply the length of the squares sides and for a circle it corresponds to the diameter.

2.2.5 Characterization of Diesel Exhaust flows

The Reynolds number is defined as:

$$Re = \frac{\rho v L}{\mu} \quad (2.5)$$

The distance needed for the development of a fully laminar velocity profile inside a channel can be determined from [23],

$$x = 0.0575 \cdot Re \cdot d_h \quad (2.6)$$

This distance is usually 5 to 50 mm for flow inside a monolith channel. For dispersed flows with particles moving in a continuous fluid the particle Reynolds number also becomes relevant:

$$Re_p = \frac{\rho v_{rel} d_p}{\mu} \quad (2.7)$$

Diesel particles are very small though and the relative velocity to the gas is low, the particle Reynolds number is therefore mostly less than one [4]. The flow regime around the particles is viscous with little oscillations in the wake of the particles. Another important parameter in particle fluid interactions is the Stokes number which relates the timescale of the particles to the fluid timescale [24].

$$St = \frac{\tau_p}{\tau_F} \quad (2.8)$$

With $St \ll 1$ the particle response time is smaller than the time for the flow field giving the particles a chance to respond to flow field changes. That is the particles will follow the flow completely and the relative velocity between the phases will be close to zero. At $St \gg 1$ the

particle trajectory is uncorrelated to continuous flow characteristics. A particle response time is given by [4]

$$\tau_p = \frac{\rho_p d_p^2}{18\mu} \quad (2.9)$$

Soot particles has a much smaller response time than the fluid system response time, the particle is thus highly dependent on the exhaust gas motion. The volume fraction of the dispersed phase is

$$a_d = \frac{\pi D^3}{6L^3} \quad (2.10)$$

Then the particles are considered to be inside a cube with distance L, which is also the distance between particle centres. A closely connected parameter is the particle spacing [25].

$$\frac{L}{D} = \left(\frac{\pi}{6a_d} \right)^{\frac{1}{3}} \quad (2.11)$$

The dispersed phase volume fraction indicates when interaction between the different phases becomes important and whether the flow is dense or dilute. A system of two phases can be considered dilute for volume fractions up to ($\alpha=10^{-3}$) corresponding to $L/d_p \approx 8$. In this regime the particles effect on the fluid is negligible and one way coupling is valid. For volume fractions $>10^{-3}$ the flow is dense and two way coupling and even four way coupling are possible. In the latter particle collisions and fluid dynamics interactions between particles must be considered in modelling [25].

2.3 Computational fluid dynamics

Computational fluid dynamics provide insight on the flow and pressure fields for both single and Multiphase flows. In the following section the most important forces acting on soot particles in exhaust gas and the particle deposition mechanisms are introduced. The equations solved for particle simulation with Euler Lagrange model and its limitation is discussed.

2.3.1 Fundamental equations

Most commercial CFD codes rely on a finite volume solver to numerically solve discretized equations for a domain divided into small computational cells. The Navier stokes equations describing the transport of fluid flow, derived over a control volume consist of the continuity equation and the momentum equations [26].

$$\frac{\partial \rho}{\partial t} + \frac{\partial \rho U_j}{\partial x_j} = 0 \quad (2.12)$$

$$\frac{\partial \rho U_i}{\partial t} + \frac{\partial \rho U_i U_j}{\partial x_j} = \frac{\partial}{\partial x_j} \left(\mu \frac{\partial U_i}{\partial x_j} \right) - \frac{\partial P}{\partial x_i} \quad (2.13)$$

Commercial CFD software first solves the momentum equation but then the demand of continuity equation is often unfulfilled so pressure and velocities must be corrected for. The pressure is solved by an iterative procedure, utilizing the following equation:

$$\frac{\partial^2 P}{\partial x_i \partial x_i} = -\frac{\partial^2}{\partial x_i \partial x_j} (\rho U_i U_j) \quad (2.14)$$

Simulating turbulence requires the addition of turbulence models to the above equations. Multiphase flows are more complex and there are many computational models available to choose from. The parameters for flow characterisation can be good aid in determining the suitable model.

2.3.2 Euler Lagrange particle tracking

Euler Lagrange simulations can be time demanding since extensive computational power is needed to compute the trajectories of each individual particle. While using a Lagrangian model one cannot simulate all the particles present physically due to the large number of particles. Instead each computational particle simulated represents a larger number of particles or a parcel of particles. Different size distributions can then be accounted for by setting parcels with a specific particle size [24].

The motion of small particles in a uniform flow with $Re \ll 1$ also referred to as Stokes flow is described by the BBO equation, based on work by Basset (1888), Boussinesq (1885) and Oseen (1927) [25]. The Lagrangian approach to describe the particle motion or trajectory in a fluid is centered on the solution of three ordinary differential equations given by:

$$\frac{dx_p}{dt} = u_p \quad (2.15)$$

$$m_p \frac{du_p}{dt} = \sum F_i \quad (2.16)$$

$$I_p \frac{d\omega_p}{dt} = T \quad (2.17)$$

Where $m_p = \rho_p d_p^3 \pi / 6$ and $I_p = 0.1 m_p d_p^2$

These equations describe the particle location, angular and linear velocities, where m_p is the mass of a spherical particle or droplet while u_p = the linear velocity [25]. The moment of inertia for a sphere is I_p and ω_p is the angular velocity of a particle and T, the torque on a rotating particle due to viscous interaction with the fluid. The particle rotation described in equation 2.17 is almost always neglected. It is not accounted for in Fluents discrete phase model, due to modeling uncertainties and high computational demand for solving rotational movement [25].

Equation 2.16 corresponds to Newton's second law and all the forces acting on the particle are considered. The forces, F_i , on the right side correspond to drag force, gravity force, pressure force, virtual mass force, Basset force, Saffman and Magnus lift force, thermophoretic force, Faxén correction force, Brownian force and turbulence.

The drag force is a function of the relative velocity between the two phases:

$$F_{i,Drag} = \frac{1}{2} A_d C_D |U_f - U_d| (U_{i,f} - U_{i,d}) \quad (2.18)$$

In this equation A_d is the projected area normal to the flow which for a sphere is equal to $\pi d_p^2 / 4$. The drag coefficient C_D depends on the shape of the particles as well as Reynolds

number [11]. The pressure and shear forces are written as a pressure and shear gradient over the particle surface, with constant pressure shear gradient over the particle volume and a particle volume fraction V_d , the following expression is valid:

$$F_{i,P} = V_d \left(-\frac{\partial P}{\partial x_i} + \frac{\partial \tau_{ij}}{\partial x_j} \right) \quad (2.19)$$

The pressure force is neglected for gas-solid flows since ρ_f / ρ_p is less than one [26]. The virtual mass force is an apparent mass force arising due to acceleration or deceleration of a fluid fraction surrounding an accelerating or decelerating particle. The added mass force is expressed:

$$F_{i,virt} = C_{VM} \rho_f V_d \frac{D}{Dt} (U_{i,d} - U_{i,f}) \quad (2.20)$$

Where V_d is the volume of the particle and the mass force coefficient, $C_{VM}=0.5$. The history force also called Basset force is due to the time required for a boundary layer to develop for an accelerating or decelerating particle. A time integral is necessary in this force due to different time scales for the particle and fluid which makes it very computational demanding, in fact calculation times may increase about a factor of 10 [26].

The Saffman and Magnus lift force is an effect of particles moving in a shear layer and experiencing a velocity gradient. A higher velocity on one side of the particle gives rise to a lift force acting in that direction, called Saffman lift force. If the particle rotates it is instead referred to as the Magnus lift force.

The thermophoretic force is a temperature gradient force, hot molecules move faster than cold molecules and a force acting opposite to the direction of the temperature gradient appears. This force is only of interest for very small particles and the same applies for the Brownian force (sub-micron particles) which is due to random collision between particles and molecules. The Faxén correction force is applied for linear gradients in fluid velocity over the surface of the particle and applies to all forces mentioned and gives high order gradients for velocity.

Turbulence is modelled as a random velocity component added to the fluid velocity. It is valid for the minimum lifetime of turbulent eddies and the time for a particle to pass through the eddy [26]. For particle motion in a turbulent field the fluid timescale corresponds to the timescales of the energy containing turbulent eddies, the time scales of turbulence, $t \approx k / \epsilon$.

The BBO equation is only valid for a few particles in a homogenous flow with small particle Reynolds number. Higher Reynolds number flows are described by the addition of an empirical coefficient to each force, a coefficient which is based on direct numerical simulations or experimental data.

2.3.3 Lagrangian point particle approach

Direct numerical simulations (DNS), a direct solution of the non-linear three dimensional Navier Stokes equations resolves the behaviour of the flow down to the smallest scales. Simulation of laminar and turbulent flows is thus described directly but at the demand of a dense grid resolution and high computational power.

In Lagrangian particle tracking, this approach can be used but most often the resolution of the flow is relaxed by applying a point particle approach instead. The particles are treated as point-wise rigid spheres, represented by source terms and possibly a volume fraction [26]. Interaction between the continuous phase and the individual particle motions is modelled with Lagrangian equations of motion, equation number 2.15-2.16. The flow of the continuous fluid is described by the single phase Navier Stokes equations here written in tensor notation,

$$\frac{\partial(\alpha_f \rho_f)}{\partial t} + \frac{\partial(\alpha_f \rho_f U_{i,f})}{\partial x_i} = S_c \quad (2.21)$$

$$\frac{\partial(\alpha_f \rho_f U_{i,f})}{\partial t} + U_{i,f} \frac{\partial(\alpha_f \rho_f U_{i,f})}{\partial x_i} = -\alpha_f \frac{\partial P}{\partial x_i} + \frac{\partial(\alpha_f \tau_{ij,f})}{\partial x_i} + S_{i,p} \quad (2.22)$$

Where α is the volume fraction of particles, S_c is as source term describing mass transfer between the dispersed and the continuous phase while $S_{i,p}$ describes the corresponding momentum exchange. All the forces in equation 2.16 except gravity, arise due phase interactions and appears in the source term $S_{i,p}$ [26]. The two equations above are valid for DNS and viscous laminar modelling but the point particle approach is applicable to both Reynolds Averaged Navier Stokes (RANS) and Large Eddy simulation models.

The point particle approach resolves the mass momentum and heat transfer around to/from each individual particle and is ideal for treating many particles. However a severe restriction is imposed by the fact that particle diameter must be much smaller than the grid spacing or computational cell. This limitation arises since the velocity U_f required for calculation of the source term and all the forces F acting on the particles, is the undisturbed fluid velocity at the centre of the particle.

The fluid velocity is obtained through interpolation from the neighbouring points and requires a grid cell size significantly larger than the particles. On the other hand accurate simulations demand a smaller grid cell than the fluid scales, if the particles are of smaller size than the smallest relevant fluid scale then the point particle restriction is fulfilled [25].

Violation of these restrictions can give significant errors for one way coupled flow where the particles do not affect the flow field. For heavy particles in gas flows with higher Stokes numbers, the inertia of the particles means that the particles are driven by the larger scales of the flow and a small grid size is not important [15].

2.3.4 Modelling of forces acting on soot particles and deposition mechanisms

The number deposition efficiency for particles deposited in a channel or pipe is governed by the forces acting on the particles and can be defined as [5]

$$E = 1 - \frac{n_{outlet}}{n_{inlet}} \quad (2.23)$$

with n representing the number concentration of particles with a specific diameter. A particle hitting a wall may either adhere or be reflected. At the walls of a catalyst agglomeration of soot particles can transpire which makes reentrainment of particles, mainly caused by vibrations and fluid shear forces, more likely [19]. Reentrainment is usually not considered in computational fluid dynamics due to modelling difficulties therefore particle trapping is somewhat overestimated.

In an aftertreatment system the important forces acting on a soot particle include the drag force, the gravitational force, the Saffman lift force, the van der Waals interaction force, electrostatic forces, the thermophoretic force and the Brownian motion described as a force [4]. The drag force is the largest force while the basset history force, the virtual mass force, the Faxén and the pressure gradient force are much smaller and therefore neglected [4]. The gravitational force or buoyancy force always acting on particles is easy to model but rather insignificant for deposition of diesel soot particles.

Particle deposition due to a thermophoretic force is a transient effect transpiring when hot exhaust gas flow through a cool substrate. For an oxidation catalyst in steady state, the effect is minor and only of interest if there is a temperature gradient in the exhaust gas phase [19]. A temperature gradient usually exists in the catalyst but for simulation purposes it is easier to assume isothermal conditions.

Electrostatic forces acting on the particles is only of interest for particles with a size of less than 100 nm and even then less than 0.5 % by mass of the total amount of particles would be removed by such a mechanism in a DOC [4].

The Saffman lift force which is due to velocity gradients, results in inertial deposition of particles but only has an effect on particle trajectories inside the viscous sublayer. The direction of the lift force is towards the walls but the equation is not valid for strong or weak shear and the presence of a wall [4].

Van der Waals interaction is an attractive force occurring between particles and walls. In CFD simulations it is possible to model it for instance between a particle and wall. The strength of the force would then depend on the wall material however the range of the force is less than a particle diameter size in nanometres hence it only affects particles very close to the wall [4].

Sub micron particles common in diesel soot are subject to random collisions with individual gas molecules which alter the particles path. This is referred to as Brownian motion. In particle simulations the Brownian movement is usually modelled as a Gaussian white noise process and is the main mechanism for collection of small soot particles.

Different sized particles in exhaust aftertreatment system are deposited by different mechanisms. The smallest particles near the size of the mean free path of the gas, approximately 10 nm, are mainly trapped by Brownian diffusion. The evidence for this in simulations is the observed random distribution of small particles on walls. Larger particles have larger relaxation times which makes them more prone to hit obstacles or promoters in a substrate channel. The inertial impact is the dominating trapping mechanism for particles > 400 nm and is an effect of particles possessing inertia and not following the gas streamlines exactly [4,19]. Another phenomenon behind particle deposition is turbulent diffusion requiring turbulence though.

3 Methods

3.1 Simulation methods

Two major computational approaches were taken to determine an uncoated monolith catalysts effectiveness in trapping soot particulate matter. One used an Euler Lagrange model, in Fluent, called the discrete phase model (DPM) which solves the Lagrangian equations of motion for particles. The major forces governing particle deposition, Brownian diffusion and drag were the only forces solved for with this model. The discrete phase model is useable for a large size range of particles since it captures both Brownian diffusion for small particles and inertial effects (particles deviating from fluid streamlines) for the larger particles.

The other approach here referred to as the species method is based on tracking tracers or species with an assigned diffusivity throughout the flow field while solving the ordinary fluid flow equations. The assigned diffusivity represented a Brownian diffusivity for a specific particle size in nm. Since Brownian diffusion is the predominant deposition mechanism for 5nm and 10 nm particles only, those sizes were expected to give accurate values in simulations with the species method. The major advantage with the species method is the faster simulation time compared to the DPM.

3.2 The Discrete phase model and UDF:s

The model chosen for tracking particles of a wide size range in Fluent 12 simulations was the discrete phase model. The flow of the gas in the domain was solved prior to injection of particles and the particles tracked in the frozen flow field, assuming one way coupling to be valid. For the discrete phase model, four user defined functions were applied to solve for drag, particle injections, Brownian motion and the time step.

3.2.1 Drag

The user defined function calculates drag and the Cunningham correlation defined as:

$$C_c = (1 + Kn_p * (2.514 + 0.8e^{(-0.55/Kn_p)})) \quad (3.1)$$

In a low pressure environment or for particles with a size in nanometres, the gas flow around the particle cannot be regarded as a continuum since the particle motion is induced by collisions of gas molecules with the particle surface [19]. The gas molecules do not stick to the particles surface instead a partial or full slip condition occurs which in turn reduces the drag coefficient. Rarefaction effects can be estimated from the ratio of the mean free path of gas molecules to the particle diameter which is the particle Knudsen number defined as:

$$Kn_p = \frac{\lambda}{d_p} \quad (3.2)$$

From kinetic theory of gases the mean free path of the gas molecules, λ is defined by:

$$\lambda = \frac{\mu_f}{0.4999\overline{c_{Mol}}\rho_f} \quad (3.3)$$

where $\overline{c_{Mol}}$ is the average relative velocity between gas molecules given by:

$$\overline{c_{Mol}} = \left(\frac{8P}{\pi\rho_f} \right)^{1/2} \quad (3.4)$$

P is the pressure of the system and at for instance atmospheric conditions with a temperature of 293 k and pressure of 1 bar, the mean free path is approximately 0.06 μ m. In the Stokes regime valid for small particles, the drag coefficient has to be reduced and corrected by the Cunningham correlation.

The user defined function calculates $\overline{c_{Mol}}$, λ and the Knudsen number and depending on the particle Reynolds number different correlations are used to obtain the drag.

Stokes law is given in the first equation below followed by different forms of correlations from [4] Morsi and Alexander.

$$C_D = \frac{1}{Cc} \frac{24}{Re_p} \quad Re_p < 0.1 \quad (3.5)$$

$$C_D = \left(\frac{22.73}{Re_p} + \frac{0.0903}{Re_p^2} + 3.69 \right) \frac{1}{Cc} \quad 0.1 \leq Re_p < 1 \quad (3.6)$$

$$C_D = \left(\frac{29.1667}{Re_p} - \frac{3.889}{Re_p^2} + 1.222 \right) \frac{1}{Cc} \quad 1 \leq Re_p < 10 \quad (3.7)$$

3.2.2 Time step

The function enforces a limit on the time step, computed in Fluent's ordinary differential equations solver, which is defined in:

$$t_{limit} = \frac{0.1 * \rho_p d_p^2 * Cc}{18\mu} \quad (3.8)$$

If the time step controlled by Fluent ordinary differential equations solver exceeds the limited value, it is set equal to the limit in equation. However if the time step never exceed the limit, it is left unmodified. Hence the time step is always smaller than the particle response time which is necessary for the Brownian force equation to be valid.

3.2.3 Body forces

The user defined function for body force, returns the real value for acceleration of particles due to the body force here Brownian motion, in m²/s to Fluent's solver. The Brownian force utilizes randomization routines to impose a random velocity component to the particle movement as it moves through the flow field and collides with other particles. A normal distributed randomized number is multiplied to the Brownian force defined by [4,27]:

$$F_{Brownian,i} = \zeta_i \sqrt{\frac{216\rho_g\nu_g k_B T}{\pi d_p^5 \rho_p^2 Cc \Delta t}} \quad (3.9)$$

T is the absolute temperature of the Fluid, ν_g the kinematic viscosity of the gas, k_B is the Boltzmann constant and Cc the Cunningham correction factor. The body force user defined function is necessary since the Brownian force in Fluent cannot use locally computed values for Cc and d_p and no size limitations exists on the time step.

3.2.4 Injection Routine

The particle injection routine sets the velocity and temperature of an injected particle equal to values from the specific cell where it was injected. The function injects particles of 12 different diameters, from 5nm to 1 μ m, the particle sizes considered is given in table 2.

Note that to obtain reliable statistical values an equal number of particles, 2000 of each particles size are injected. The normalized number concentration can be used to account for the correct number distribution of particles of different sizes in the final result.

The soot particle density assumed was 1000 kg/m³ for the whole particle size range. In reality the PM will have minor differences in density and the classification of particulate matter is difficult therefore this assumption is still good. In all simulations only one way coupling between the particles and the exhaust gas is accounted for, therefore the flow affects the particles but not the other way around.

PM type	Particle diameter (nm)	Normalized number concentration
Small particle in nuclei mode	5	0.0241
Typical particle in nuclei mode	10	0.3131
Typical particle in nuclei mode	20	0.5010
Large particle nuclei/accumulation mode	30	0.0722
Large particle nuclei/accumulation mode	50	0.0144
Large particle nuclei/accumulation mode	100	0.0289
Typical particle in accumulation mode	150	0.0193
Typical particle in accumulation mode	200	0.0120
Large particle accumulation mode	250	0.0096
Large particle accumulation mode	300	0.0048
Large particle accumulation mode	500	0.0005
Particle in coarse mode	1000	-

Table 2: Particles of different diameters used in CFD simulations, the normalized number concentration and classification of particulate matter was obtained from [4].

3.3 The Species method

Particle simulations with the Euler Lagrange discrete phase model can be time demanding since it requires extensive computational power to compute the trajectories of each individual particle. Therefore a method to screen the particle trapping efficiency for different catalyst designs was applied.

Since Brownian diffusion is the predominant mechanism for deposition of particles on catalyst walls, at least for small particles with diameters of 5-10 nm. It is possible to simulate tracers or species released from the inlet of the channel which are assigned a Brownian diffusivity representative for a specific particle diameter (see table 3). A user defined function where the diffusivity of each species is set according to the table was applied. The exhaust flow to be simulated in CFD simulations will then be represented as a mixture of air and six different species. The physical properties of the species are set to the same value as air at 300°C.

Species	Particle diameter (nm)	Brownian Diffusivity (m ² /s)
A	5	8.337* 10 ⁻⁷
B	10	2.100* 10 ⁻⁷
C	100	2.390* 10 ⁻⁹
D	150	1.137* 10 ⁻⁹
E	500	1.535* 10 ⁻¹⁰
F	1000	5.848* 10 ⁻¹¹

Table 3: Brownian diffusivities assigned as a diffusivity for different species in a user defined function, at 300°C and atmospheric pressure.

The distance covered for a particle by Brownian diffusion, the root square displacement is defined as:

$$\Delta x = \sqrt{2Dt} \quad (3.10)$$

$$\text{Where } D = \frac{k_B T C_c}{2\pi\mu d_p} \quad (3.11)$$

The diffusivity in table 6 was calculated with latter equation. The boundary conditions here were set to a 1 % mole fraction of each species on the inlet and to zero mole fractions at all the walls. The result was reported as a trapping efficiency, E:

$$E = 1 - \frac{\text{Mole fraction outlet}}{\text{Mole fraction inlet}} \quad (3.12)$$

where the mole fractions are mass weighted averages.

3.4 General conditions and boundary conditions

The exhaust gas simulated where given the same conditions as air at 300°C: a dynamic viscosity of $\mu=2.93 \cdot 10^{-3}$ and density of $\rho = 0.61 \text{ kg/m}^3$. A viscous laminar model was used with Fluents discrete phase model and the user defined functions described above to account for soot particle motion. Transient thermal effects such as thermophoresis and temperature gradients were neglected and isothermal conditions assumed.

The standard velocity inlet boundary condition was used with a velocity of 10 m/s and a pressure outlet boundary condition. A laminar velocity profile is expected to be developed after 5 mm in the monolith channel therefore the first promoter was always positioned at least 10 mm from the inlet. The distance from the last promoter and channel outlet had to be a minimum of 20 mm to avoid convergence difficulties due to large variation in the velocity profile.

The wall boundary conditions was set to instant trapping for particle simulations, the position of all particles injected in to the channel were then obtained once they encountered a wall or moved through the outlet. Each particle hitting a wall was considered trapped in the catalyst, reflections and reentrainment effects were not considered. All the simulations on the catalysts where made in three dimensions with double precision.

3.5 Simulation of forces acting on a particle in a vortex

From simulations of the gas flow in the monolith channels with promoters it was noticed that two vortices formed after the obstacle. See the velocity vectors over the outlet, given in figure 19B. This flow pattern is similar to the one found by Andersson and Schöön (1993) for flow in sinusoidal channels with obstacles and has been experimentally verified [28].

It is possible to estimate how strong vortices (angular velocities) created with promoters need to be for particles of twelve different sizes to deposit on the catalysts walls. To determine the angular velocity in radians/second needed for a vortex to transport a particle out to the wall during a time τ , a system of two differential equations must be solved:

$$\frac{dr_p}{dt} = u_p \quad (3.13)$$

$$\frac{du_p}{dt} = \frac{1}{m_p} (F_{CF} - F_D) = -\frac{18\mu u_p}{d_p^2 C_c \rho_p} + \omega^2 r_p \quad (3.14)$$

The first solves the derivative of the radial position for a particle in a vortex which is the particle velocity and the second equation calculates the particle acceleration from the centrifugal and drag force. The centrifugal force acts outwards from the centre of a vortex while the drag acts in opposite direction to decrease the particle movement. The drag and centrifugal force are given in equation 3.15 and 3.16 respectively.

$$F_D = \frac{\pi d_p^2}{4} C_D \frac{\rho_g u_p^2}{2} C_c \quad (3.15)$$

$$F_{CF} = m_p \omega^2 r_p \quad (3.16)$$

The right side of equation 3.14 is obtained from the expression for drag and centrifugal force and by setting the drag coefficient as in equation 3.5, thus assuming stokes drag.

Here ω^2 is the angular velocity in radians/second and r_p is the radial position of the particle. The mean axial flow velocity in the monolith after the obstacle was assumed to be 20 m/s and the distance from the obstacle to the outlet 20 mm. Therefore the average retention time here denoted τ for a particle following the mean flow is 1 ms. At that time a particle affected by a vortex has to have reached the monolith wall to be considered trapped in the system.

The monolith channel width corresponded to 2 mm, therefore the vortex radius was set to 0.5 mm and a cylindrical coordinate system with coordinate zero in the vortex center applied. Assuming an initial particle position at 0.25 mm from the wall and also from the center of the vortex, the angular velocities required for particles of the twelve different sizes to reach the wall were calculated. The differential equations were solved with the software Matlab, assuming initial conditions: zero radial velocity for the particle and position $2.5 \cdot 10^{-4}$ m.

3.6 Geometry 1: monolith channel with promoter

The first geometry simulated consisted of a monolith channel with a promoter introduced to improve particle deposition on the walls. The first obstacle created had a similar geometry as the one in studied by Andersson and Schöön [12] but it was decided to place it in a square formed monolith instead of a sinusoidal. Then CFD simulations on automotive exhaust gas flowing through the channel, would give insight on the flow pattern or vortices generated by the obstacle.

The geometry used in simulations consisted of a monolith channel with a height and width of 2 mm. With the obstacle in the channel, the channel length varied from 32.09 mm to 35.33 mm since it depended on the obstacle length. The promoter and monolith channel simulated is given in figure 7.

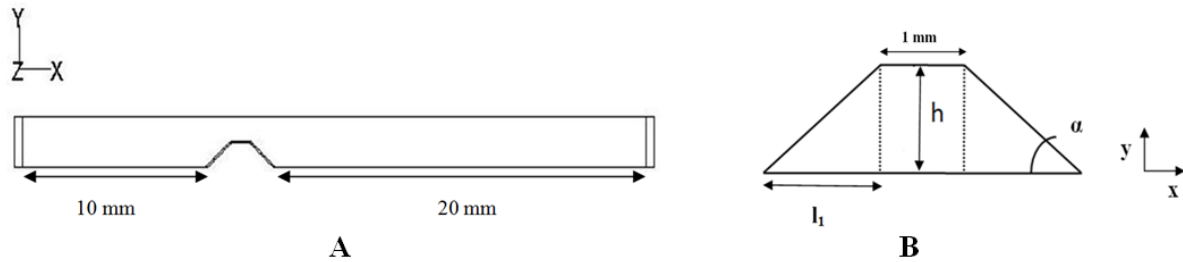


Figure 7: A: Monolith channel of geometry 1, B: promoter and parameters considered in the setup.

To study how the pressure drop and particle trapping efficiency in the monolith, depend on the shape of the promoter, two factors (the angle α and the height h) of the promoter were examined at three levels (see table 3).

Case	Height h (mm)	Length l_1 (mm)	Angle α ($^\circ$)
0	0	0	0
1	0.75	1.299	30
2	0.75	0.833	42
3	0.75	0.545	54
4	1.0	1.732	30
5	1.0	1.111	42
6	1.0	0.726	54
7	1.25	2.165	30
8	1.25	1.388	42
9	1.25	0.908	54

Table 4: Simulation setup for the first geometry.

3.7 Geometry 2: monolith channel with four promoters

The second geometry consisted of a channel with four promoters, all with a 54° angle on the surface against the flow and a surface area of 1.5 mm^2 , each covering 37.5% of the channel cross sectional area. The two first obstacles were based on the optimal height 0.75 mm and angle 54° for a single promoter in a monolith channel (see results geometry one).

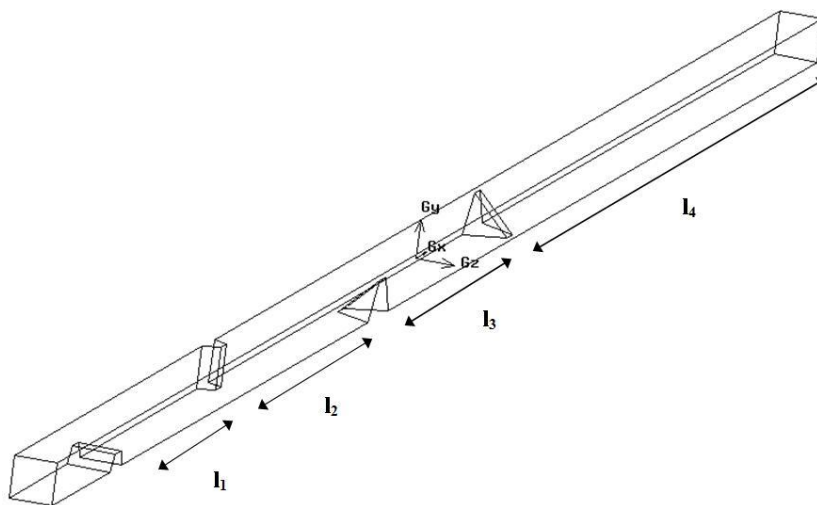


Figure 8: Geometry 2, a monolith channel with four promoters

The distance to the first promoter was 10 mm and the remaining lengths altered according to the values in table 4.

Case	Length l_1, l_2, l_3 (mm)	Length l_4 (mm)	Total length (mm)
2.0	-	-	131.212
2.1	20	50	131.212
2.2	25	35	131.212
2.3	30	20	131.212

Table 5: Simulation setup: two different types of promoters were added, promoter 1 and 2 had a length of 2.09 and 3.516 mm.

All the cases were also tested with different inlet flow velocities: 5, 10 and 15 m/s. The four promoters were placed to create a rotational flow or swirling flow so fluid elements would be exchanged and particles deposited on the walls due to the formed vortices. The expected flow pattern can be viewed in figure 9 and should be compared to the velocity profiles for planes placed 10 mm behind the promoters, see figure 22-23.

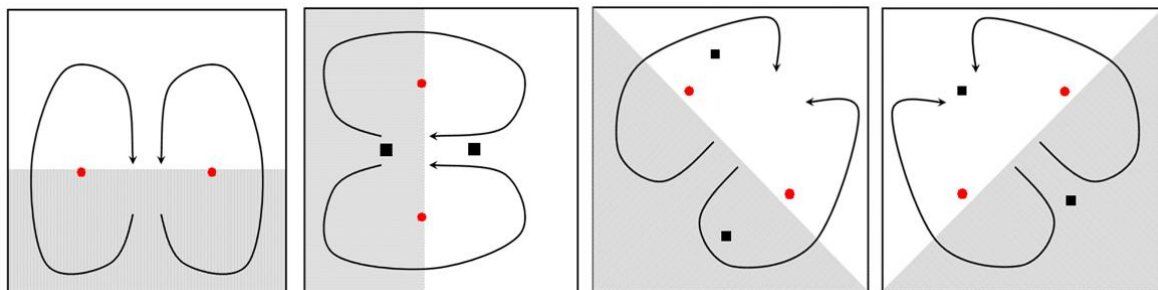


Figure 9: Flow loops in sequence. Expected flow pattern observed downstream from the obstacle (shaded grey). The arrows indicate the fluid motion after the obstacle. Red circular dots indicate centers of fluid rotation and black square boxes indicate where the previous centers of fluid rotation were positioned.

3.8 Geometry 3: monolith channel with planes

The third geometry was a 180 mm long channel covered with 18 planes with a height of 50 μm . The channel height was 2 mm while the width was set to 1 mm since a symmetry plane were used in the middle of the channel to reduce the total number of cells.

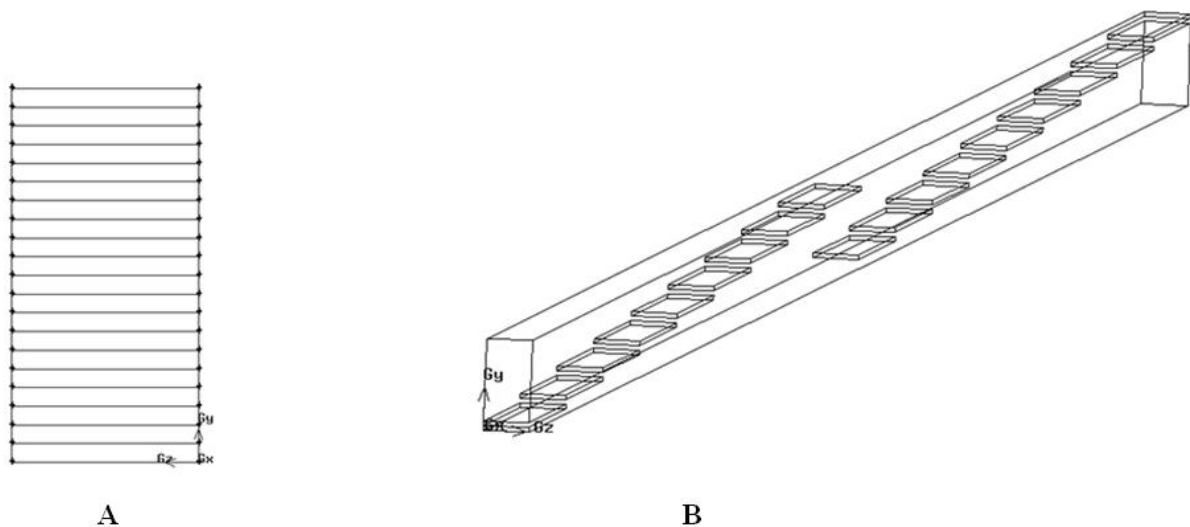


Figure 10: Geometry 3: A: View from the inlet, B: From the side displaying the 18 plates.

The purpose of introducing planes in the channel was to improve the particle trapping efficiency by considering the distance covered for a particle by Brownian diffusion, the root square displacement. In appendix A1 an estimation of the plate length needed to trap a specific particle size is given.

The effect of the displacement is short and thus another option is to cover the cross sectional area visible from the inlet with plates. Then the number of plates will be $(1 \text{ mm} - 2 \cdot 50 \mu\text{m}) / (50 \mu\text{m}) = 18$ plates. With a total length of 180 mm each plate is allowed to be 10 mm long.

3.9 Geometry 4: monolith channel with tortuous path

The fourth and last geometry was based on a commercially available catalyst. Since no data regarding particles deposition for this catalyst was found in the literature [12] it was decided to test such a configuration. The main design parameter of interest was the angle α and to test if a steeper angle potentially would give higher trapping of larger particles due inertial effects. The design is given in figure 13, the height and width, z and y direction was 2 mm and $h=1.25$ mm.

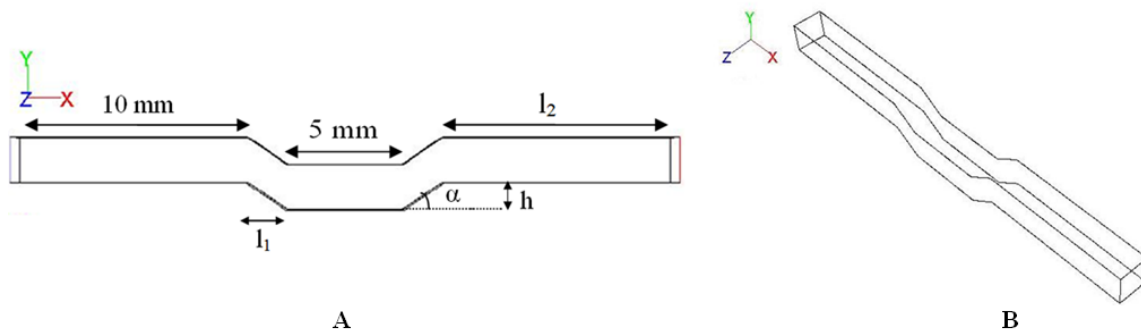


Figure 11: Geometry 4, Left: 2D view and parameters considered in the simulation setup, Right 3D.

The parameters altered in the study believed to affect the pressure drop and particle trapping efficiency, are shown in table 5 below.

Case	Angle α ($^\circ$)	Length l_1 (mm)	Length l_2 (mm)	Total length (mm)
4.0	-	-	10	28.42
4.1	35	1.71	10	28.42
4.2	45	1.2	11.02	28.42
4.3	55	0.84	11.74	28.42

Table 6: Geometry 4 a catalyst with tortuous path

3.10 Geometry 5: Porous promoter

The possibility to reduce the pressure drop and increase particle trapping has been studied through the use of porous promoters with different permeability. In the simulations a single 32 mm long channel was used with a porous promoter of height 0.75 mm and angle of 54° corresponding to case 3 for geometry one. The boundary conditions applied was viscous resistance specified according to table 13 for x, y and z directions and with a mass fraction of zero in the promoter and channel walls for specie A and C.

In laminar flows through porous media, the pressure drop is proportional to velocity. Fluent models flow in porous media with a source term, providing a sink to the Navier Stokes equations. The source term consists of both a viscous loss term an inertial loss term:

$$S_i = \frac{\mu}{\alpha} v_i + c_2 \frac{1}{2} \rho |v| v_i \quad (3.17)$$

The second term representing the inertial loss is neglected since convective acceleration and diffusion not considered, the remaining equation is Darcy's law:

$$\Delta P = -\frac{\mu}{\alpha} \vec{v} \quad (3.18)$$

The amount of specie A and B on the walls was determined for 6 different permeabilities.

3.11 Mesh

The mesh required varied widely depending on the simulation setup and geometry to be simulated. In general the mesh was created in Gambit with further refinements made in Fluent. The first geometry simulated had a basic hexahedral mesh with a spacing of 0.1 mm and approximately 130 000 cells for each case simulated. Since particle injection was based on surface, with particles injected in 400 equally sized inlet faces, further refinement of the mesh along the walls could not be made for the first simulation series. Note that for all other simulated geometries other injection routines gave no restrictions in the number and size of the inlet cells.

For the second setup with four promoters in a channel a tetrahedral mesh with spacing 0.3 mm was created with the T-grid scheme. A size function with a growth factor of 1.5 for a start spacing of 0.1 mm up to maximum of 0.3 mm was applied. The result was better resolution from the walls and into the volume space of the channel, the total number of cells reached 1 200 000.

The third geometry consisting of planes was a complex geometry to mesh with the accuracy of the solution depending on the grid size. Even with a reduced channel width, through the use of symmetry planes over 1 200 000 cells was needed. The refinement of the first mesh in specific areas can be observed in the following figures.

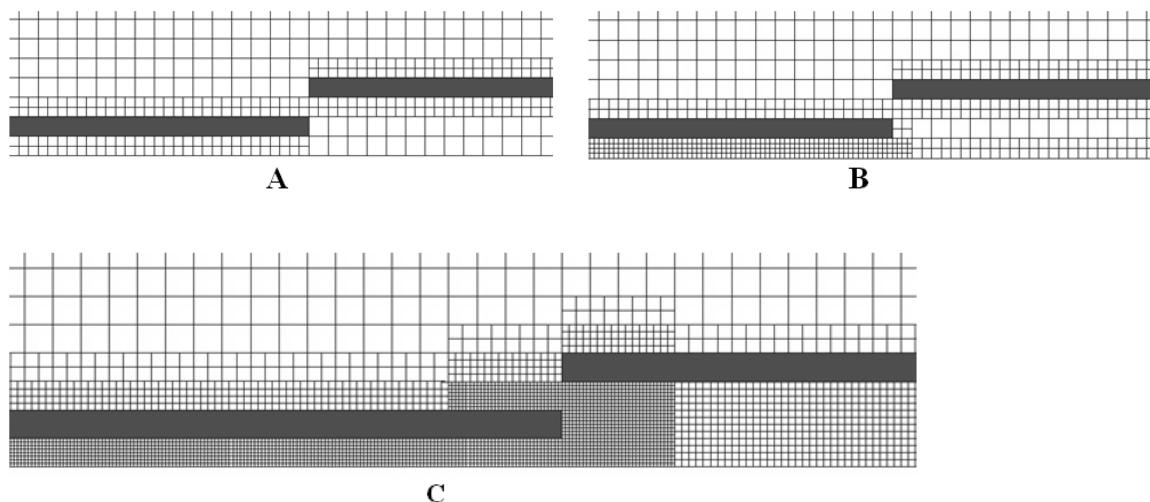


Figure 12: Geometry 3 refined mesh near the planes, A case 3.1 with 1.2 million cells, B: case 3.2 with 1.5 million cells, C: case 3.3 with 4 million cells.

The fourth alternative setup had a cooper scheme mesh with 0.08 mm in spacing for the hexahedral elements and the number of cells reached 600 000. The first cell layer closest to the wall was adapted in Fluent, giving a fine boundary layer with smaller cells and the velocity gradient was also further refined. These measures gave better resolution for swirling flows, recirculation zones and large gradients near walls.

Some of the measures applied to improve the mesh were: refinements of velocity gradients, increased resolution in specific areas of the geometry as well as boundary layer adaption and the use of size functions. The parameters available indicating mesh qualities were checked for each mesh in Fluent, the equisize skew was always less than 0.98 and the aspect ratio below 5.

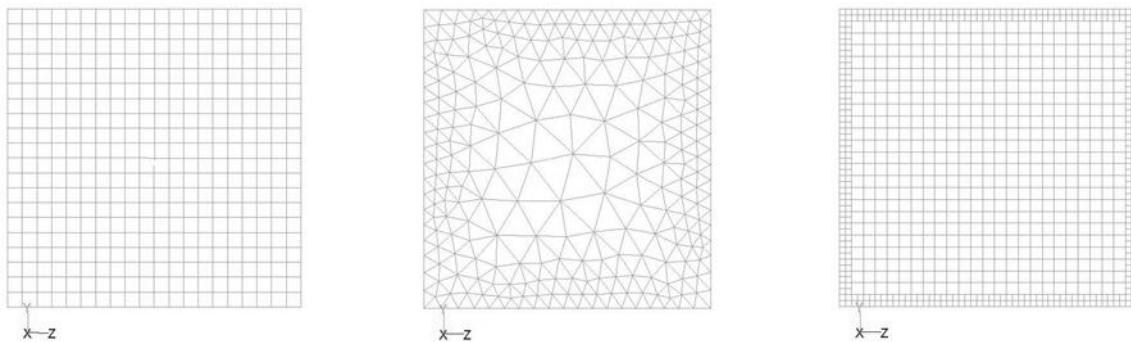


Figure 13: From left to right: Inlet face mesh on geometry one no adaption, geometry two with size functions applied and geometry three with adapt boundary layer first cell layer.

3.12 Convergence Criteria

The main numerical scheme used was the Quick scheme which provides good accuracy for the rotational and swirling flows encountered here. Another benefit is the reduced numerical diffusion compared to the first order upwind scheme. However in cases where convergence could not be obtained, a first order upwind solution was applied

Quick is third order accurate and will typically be more accurate on structured grids aligned with the flow thus reducing the numerical diffusion. For quadrilateral and hexahedral meshes, the flow can merely be aligned with the grid in simple flows for instance pipe flow. Since that can never occur for like triangular or tetrahedral grids that is in general for hybrid grids or unstructured grids, Quick instead uses a 2nd order discretization for such [29].

The convergence criteria were set to 10^{-6} for the scaled residuals even though that criterion was mostly never fulfilled for the species residuals. In general the convergence was not solely determined from the value of the residual itself but rather from its behavior. Before concluding that a converged solution had been reached, the residual had to continuously decrease or remain at a constant low value for several hundred iterations. To confirm the existence of steady states solutions, transient simulations were also performed with the demand that different parameters must converge on a constant level.

4 Results

4.1 Particle movement in a Vortex

Solving the equation of motion, centrifugal and drag equations gives the result plotted in figure 14 for the movement of particles in a vortex. The response time for a 5 nm particle is roughly 9.5 ms and for a 1000 nm particle 1.89 s

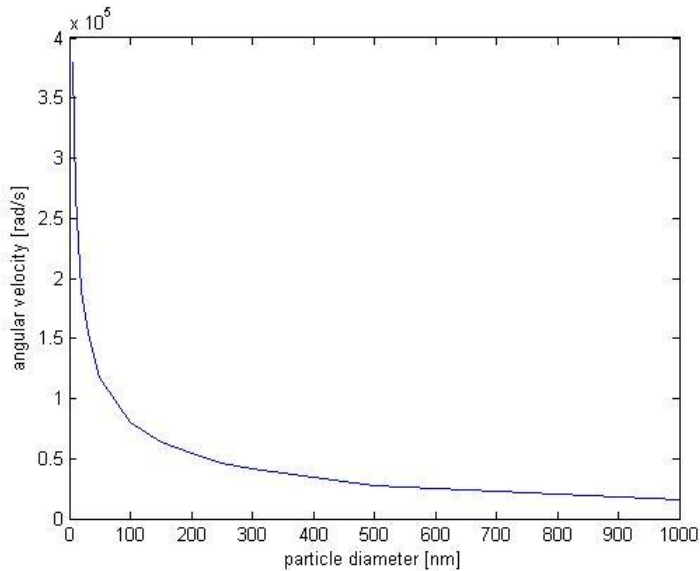


Figure 14: Angular velocity in radians/s required for particles to move 0.25 mm in radial direction in a vortex and thereby hit a monolith channel wall. Calculation based on the assumption of a particle retention time of 20 ms.

The results in figure 14 should be compared to values obtained from Fluent for the different promoters which were in the range of 5000-10000 radians/s. The values created with promoters are thus at least 10 smaller than the required for particles to move 0.25mm during 1 ms and deposit on the catalyst walls. It should be noted that the angular velocity is twice the vorticity a more common term in fluid dynamics calculations defined as the curl of a vector field. If w is the vorticity and v the velocity the following expression is valid.

$$\vec{w} = \vec{\nabla} \times \vec{v} \quad (4.1)$$

4.2 Results for Geometry one

The results from DPM particle simulations on geometry one is given in figure 15 and for the optimal case corresponding to a height of 0.75 mm and an angle of 54° in table 7. The result of the entire series, (see figure 15) was that promoters with height, 1-1.25 mm provide better trapping with smaller angle while the opposite occurred for 0.75 mm. Evaluation of the trapping efficiency was performed with equation 2.23, particles trapped in the inlet are not considered in the trapping efficiency.

The only particles trapped to any significant extent for all cases is the 5 nm particles with an optimum of 9.72 %. This value should be compared to the percentage obtained in an empty channel of the same length which is 5.65%. For exact values of the number of particles deposited in the channel with promoters and empty channels of equal length see appendix A4.

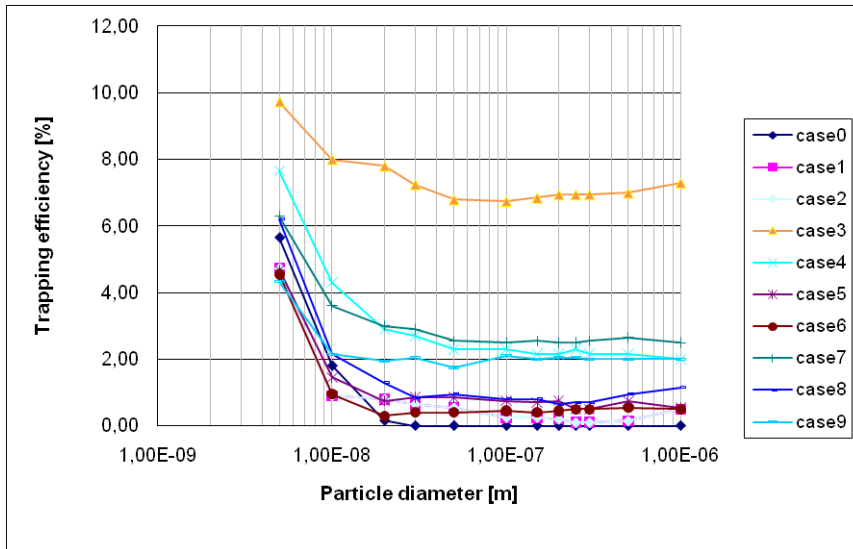


Figure 15: Diagram displaying the results from the DPM particle simulations.

The remaining particle sizes are not deposited to any extent in the channel since Brownian diffusivity is an insignificant trapping mechanism for them. With the species method there were no significant differences between particle trapping efficiency for 5 and 10 nm particles for an empty channel and all the nine cases with promoters simulated.

Dp	% trapped DPM case 3	% trapped case 0	% trapped species case 3	% trapped case 0
5 nm	9,72	5,65	5.45	5.45
10 nm	8,00	1,80	2.23	2.23
20 nm	7,80	0,15	-	-
30 nm	7,25	0,00	-	-
50 nm	6,80	0,00	-	-
100 nm	6,75	0,00	0	0
150 nm	6,85	0,00	0	0
200 nm	6,95	0,00	-	-
250 nm	6,95	0,00	0	0
300 nm	6,95	0,00	-	-
500 nm	7,00	0,00	0	0
1000 nm	7,30	0,00	0	0
Total nr	=24000			

Table 7: Euler Lagrange simulation with Fluent’s discrete phase model (DPM), 24000 particles injected in the inlet, species method – represents not simulated, case0 corresponds to an empty channel.

The pressure drop in the monolith channel is displayed in table 8 and generally increases with the height of the promoter and angle of the surface aligned towards the flow. Convergence difficulties were encountered when solving the flow for case 8 and 9 where the promoters reached 1.25 mm in height of the total channel height 2 mm and the angles 42 and 54°. Since the two promoters for those cases covers 62.5% of the cross sectional area, a high axial velocity after the promoter is produced and the velocity profile is not fully developed at the outlet (see figure 16).

Case	Pin (Pa)	Pout (Pa)	ΔP	%
0	101466	101325	141	-
1	101509	101325	184	30
2	101514	101325	189	34
3	101524	101325	199	41
4	101510	101325	185	31
5	101509	101325	184	30
6	101514	101325	189	31
7	101517	101325	185	31
8	101615	101325	290	101
9	101623	101325	298	106

Table 8: Obtained pressure from simulations, % column is the increase in pressure compared to the empty channel.

To avoid convergence difficulties a channel with an extended length of 20 mm added to the distance from the promoter to the outlet was simulated. Then from the converged solution obtained, interpolation data were applied for the standard case 8 and 9. Despite this measure only 1st order upwind scheme solutions converged.

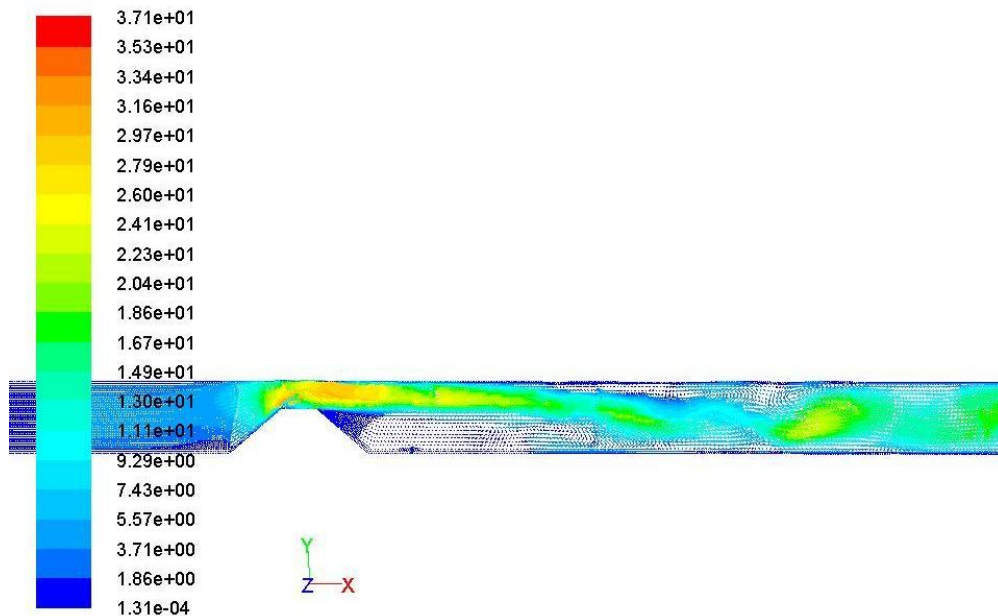


Figure 16: Velocity vectors m/s case 8 refined mesh on velocity gradients.

The position of particles in the channel outlets was investigated through plots with the software Paraview. Unfortunately it was difficult to find any trends even if only particles of one diameter were observed in the outlet. In figure 17A though it can be seen that small 5 nm particles tend to be spread all over the outlet plane which indicates that the Brownian motion is a significant effect for those. Larger particles are spread in smaller extent over the outlet since they possess inertia and do not follow the flow streamlines exactly.

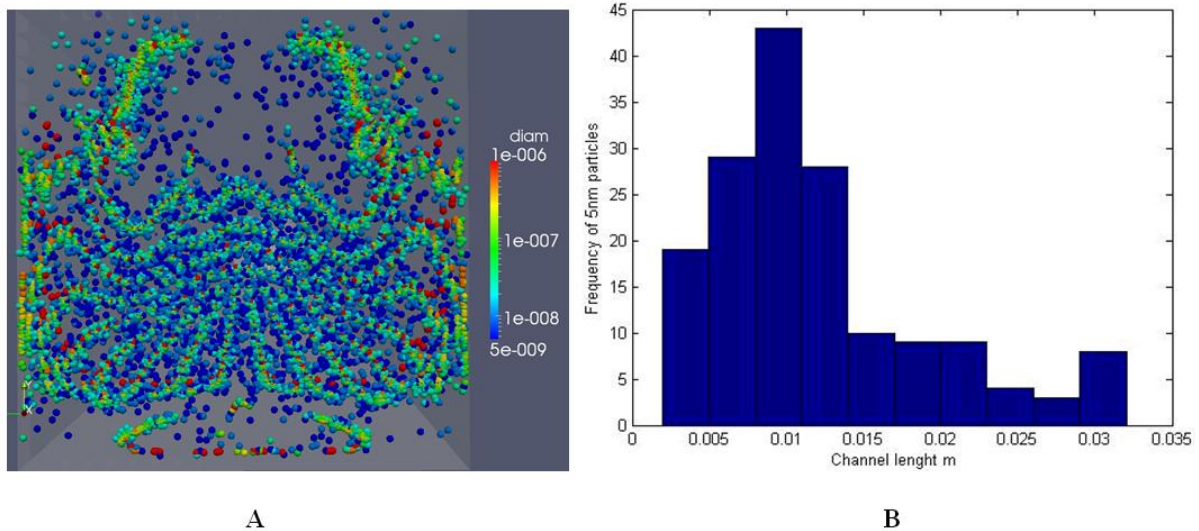


Figure 17: A: Outlet case 3, Particles with diameters in the range of 5nm-1000nm created with ParaView 3.4.0. B: Histogram plot channel length plotted versus 5 nm particle collected on the walls.

Observing where most of the 5 nm particles end up on the walls, through a plot of their x coordinates versus the number of particles in a histogram plot, see figure 17B. Seem to indicate that most particles hit the front and the top of the obstacle directly, (the edge of the promoter is at position 0.01 m).

Since the injection method for particles with the DPM method was based on surface for simulations on geometry one, no refinements of the mesh were made. For comparison of results between the discrete phase model and the species method the same mesh were applied for both methods, without any refinement. The standard mesh of 130 000 cells was near grid independent which can be seen in table 3. The refined mesh had better resolution on the largest velocity gradients and near the walls.

Mesh size	130 000 cells		511 000 cells	
	A	B	A	B
Specie				
Mole fraction Inlet	0.009998	0.009999	0.009998	0.010000
Mole fraction Outlet	0.009419	0.009808	0.009419	0.009752
E (%)	5.52	1.91	5.796	2.477

Table 9: Grid test on case 3, spacing 0.1 mm. E= trapping efficiency in %.

The mole fraction of specie A in case 3 both for the standard and refined mesh (figure 18) clearly show that most of the tracer specie A follow the core flow. Only a small amount is deposited on the walls, a better resolution of the cells near the walls, figure B proves that the boundary condition, zero mole fraction near the wall is fulfilled.

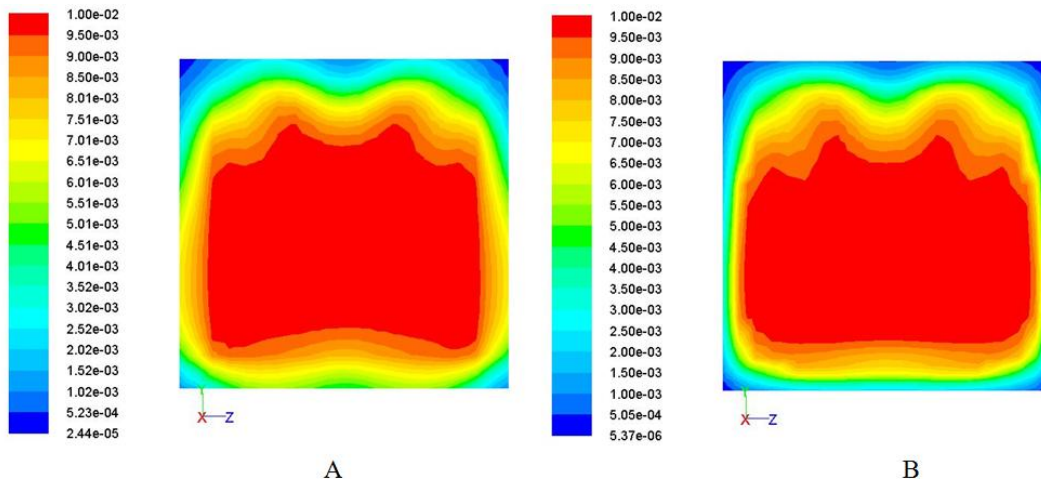


Figure 18: A: Mole fraction of specie a in the outlet for case 3, B: same but for a refined mesh.

The species method did not confirm case 3 as an optimum. Instead the highest values were achieved for case 8 and 9 with the 1st order upwind scheme, approximately 6% trapped of species A and 2.5 for species B. However since numerical diffusion occurs and the empty channel has trapping efficiencies very close to those values, no differences between different promoters can be concluded.

The recirculation zones formed after the promoter were clearly visible for all cases but more developed for case 8 and 9, (figure 19) which also had the highest axial velocities after the promoter of all cases. The outlet velocity vectors show two vortices 20 mm after the single promoter.

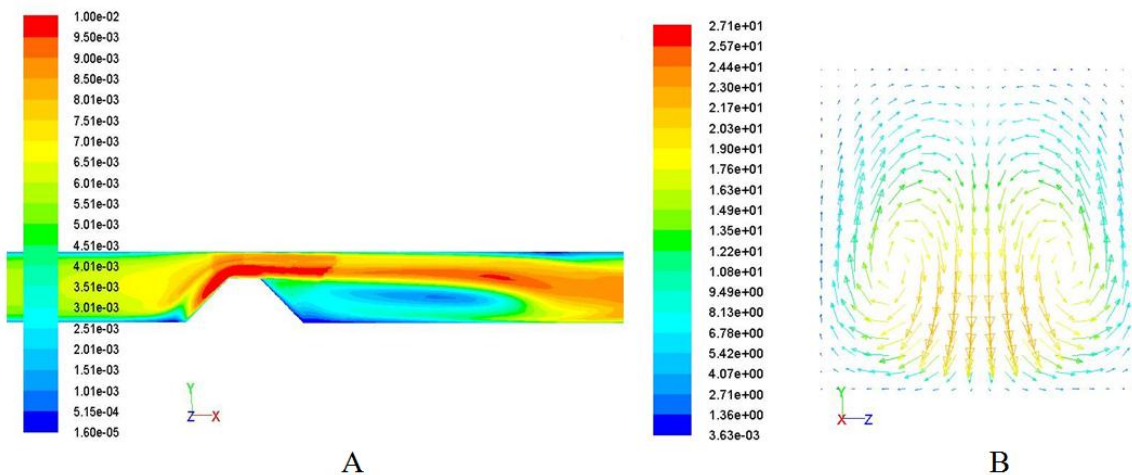


Figure 19: A: Mole fraction specie A case 8, the blue area is the recirculation zone formed after the promoter. B: velocity profile in the outlet.

4.3 Results for Geometry two

The simulation setup for the channel with four promoters aimed at finding differences in trapping efficiency based on the distance between the promoters. The species method gave only minor differences in effect of trapping efficiency for the different lengths between the promoters. The optimum was 20 mm between the promoters corresponding to case 2.1. The dense and refined mesh applied required the use of other injections routines than the surface based for the DPM simulations. However because of the long simulation time required, only one case was tested with the discrete phase model, case 2.1. Particles were injected in groups of 400 evenly on the inlet boundary (for details on injection routines see appendix A2).

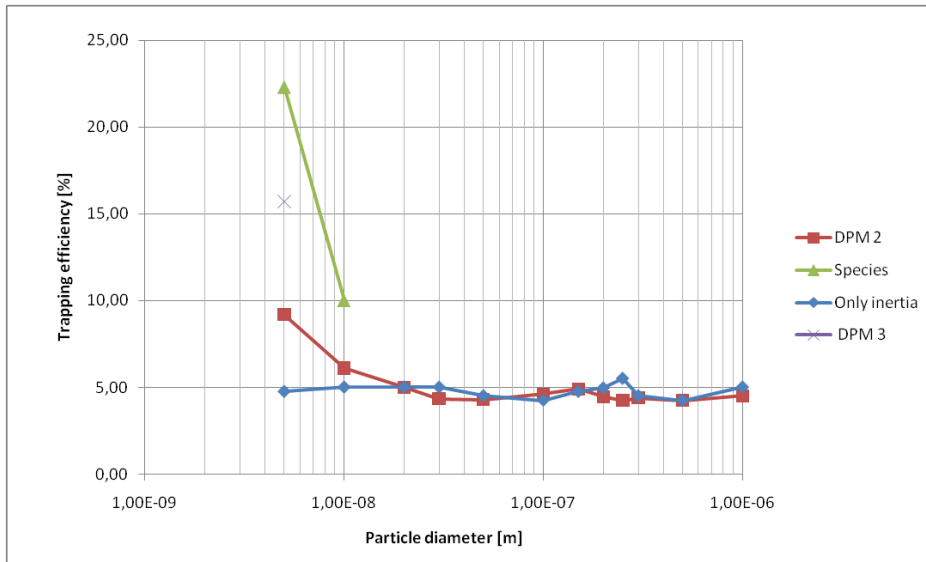


Figure 20: Trapping efficiency case 2.1 (20 mm distance between each promoter) DPM 2 and 3 are discrete phase model simulations with two different injection routines, routine 2 and 3.

The low trapping efficiency especially for the 5 nm particles obtained tend to indicate that position of injection for the particles affects the result. It is clear by comparing DPM 2 with DPM 3 that nearly twice the amount of 5nm particles are trapped, 16% instead of 9%.

Running case 2.1 with Brownian diffusion turned off resulted in fewer 5 nm and 10 nm particles trapped which is logical since the Brownian force is more developed for those. The differences between the other particle diameters were small which is due to small Brownian diffusivity of larger particles.

4.3.1 Transient simulation case 2.1

To confirm the existence of a steady state solution for the channel with four promoters, a transient simulation was performed with a time step of 1 μ s. The outlet mole fraction of specie A and inlet pressure were monitored against the actual flow time and time step, in both diagrams a stable level is reached, proving the existence of a steady state solution. The outlet mole fraction of species A converged on a value of 0.0072 with an inlet mole fraction of 0.01 thus 28 percentage particle trapping is reached. The inlet overpressure is 475 Pa and gives a pressure drop 50 percent higher than for an empty channel. The values obtained for species trapping and pressure drop are similar for those of a steady state simulation.

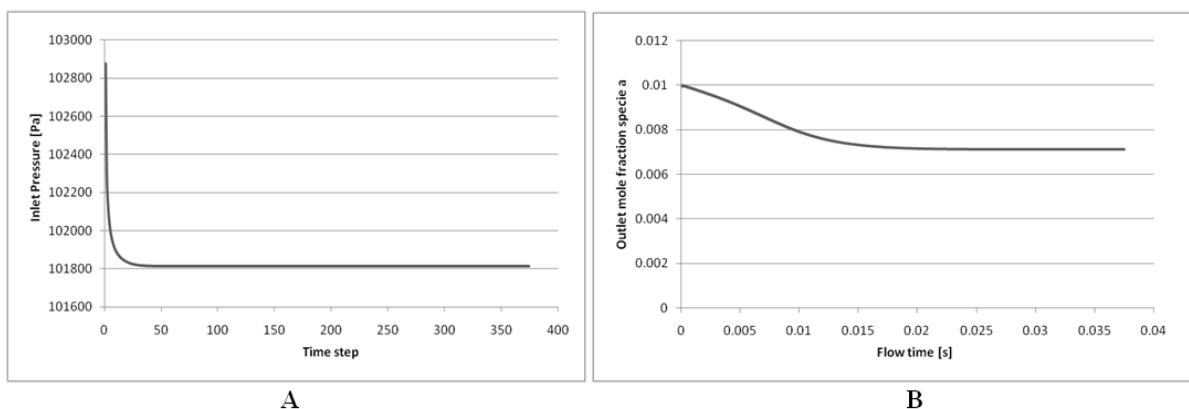


Figure 21: Transient simulation case 2.1, A: Inlet pressure versus time step. B: Outlet molefraction versus actual flow time.

4.3.2 Flow velocity effects

Since the solution here is nearly grid independent due to the fine mesh, the species method was deemed accurate to predict trapping of 5 and 10 nm particles. The results support the argument that small particles are trapped to a larger extent if the gas velocity decreases from 15 m/s down to 10 and 5 m/s. This due to the added particle retention time, meaning that longer distances can be covered by Brownian diffusion. Higher gas velocities also increase the probability that a particle will not respond to changes in gas flows fast enough to avoid hitting a promoter.

v=10 m/s	ΔP	% increase	E Spec A	E Spec B
Case 2.0	316.36	-	10.10	4.28
Case 2.1	470.66	48.77	22.32	10.01
Case 2.2	471.09	48.91	22.14	9.92
Case 2.3	472.98	49.51	22.22	9.91
v=5 m/s				
Case 2.0	146.91	-	15.10	6.48
Case 2.1	196.95	34.06	28.85	14.38
Case 2.2	197.01	34.10	28.66	14.24
Case 2.3	197.39	34.36	28.84	14.34
v =15 m/s				
Case 2.0	507.77	-	8.679	3.357
Case 2.1	816.27	60.76	19.159	7.756
Case 2.2	816.07	60.72	18.989	7.677
Case 2.3	819.82	61.45	18.952	7.622

Table 10: Pressure data at different velocities, % is the increased pressure drop compared to an empty channel, case 0. E = trapping efficiency in %.

The velocity profiles obtained on a plane perpendicular to the flow, 10 mm after each promoter is in accordance with the expected pattern.

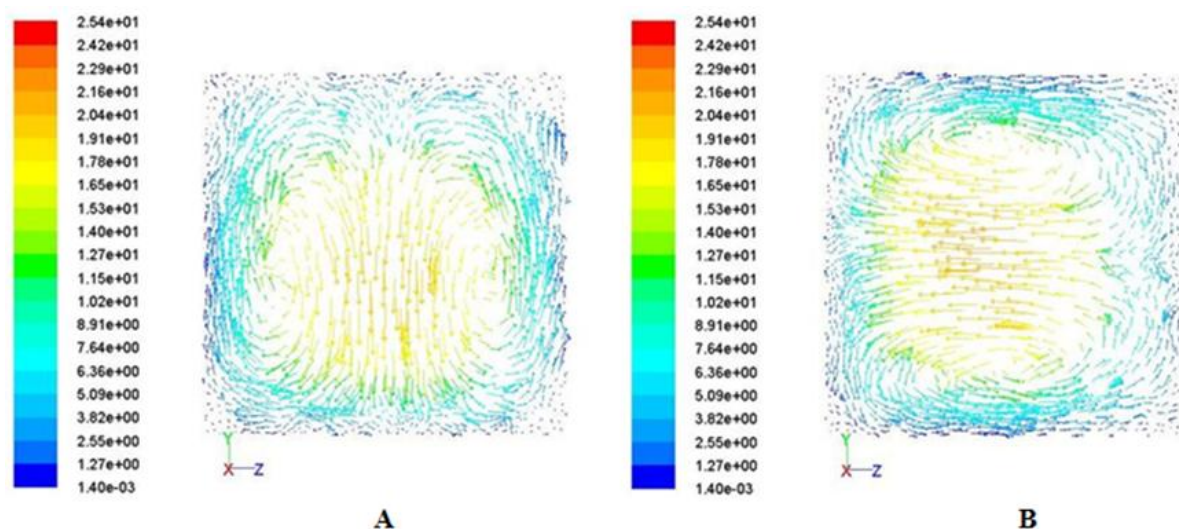


Figure 22: Velocity vectors m/s 10 mm after A: first promoter, B: Second promoter.

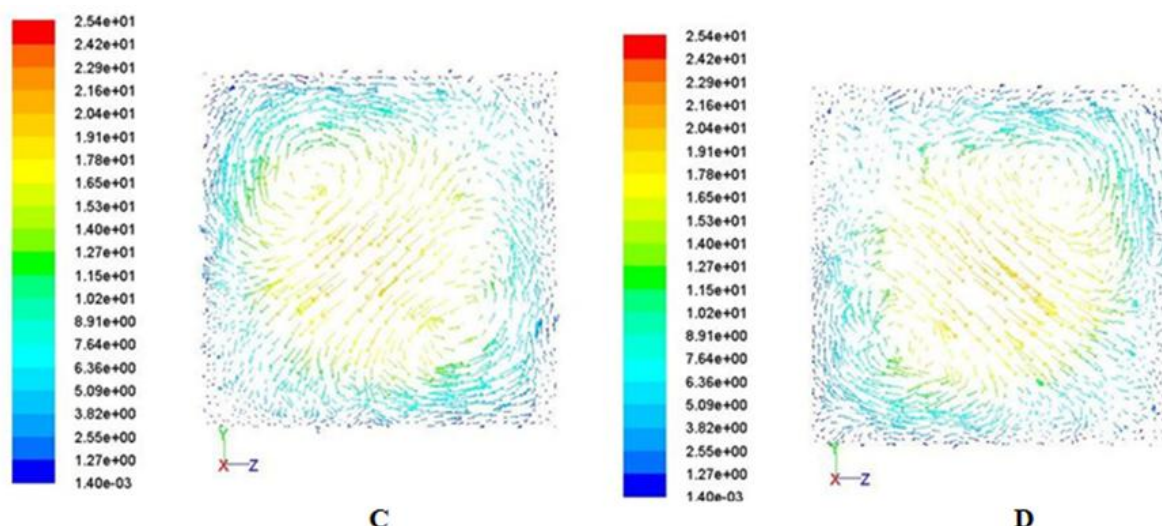


Figure 23: Velocity vectors m/s 10 mm after C: Third promoter, D: Fourth promoter.

4.4 Results for Geometry 3

The third geometry was demanding to mesh since areas between the planes and walls required refinement and there was also a restriction on the maximum number of cells that could be simulated at reasonable simulation times. The solution is not independent of the grid applied. Case 3.3 with a mesh of roughly 4 million cells is the most accurate with a trapping efficiency for specie A reaching 68.3 % but at the expense of a high pressure drop. Running discrete phase model simulations for the third geometry was not an option due to inaccurate solution, the species method provides better accuracy for 5 and 10 nm particles.

Case	Cells	Particle a	Particle b	Particle c	Particle d	Particle e	Particle f	ΔP
Refined 3.1	1.216000	63.6%	35.1%	1.37%	0.68%	0.096%	0.037%	4221.38 Pa
Refined 3.2	1.468630	63.5%	35.1%	1.42%	0.71%	0.10%	0	4394.27 Pa
Refined 3.3	4.061920	68.3	-	-	-	-	-	4557

Table 11: Grid test on geometry 3 with species method.

4.5 Results for Geometry 4

The results for the fourth simulation series is presented in tables and figures below, here the trapping efficiency and pressure drop increases with the angle α from 35-55°. Hence there is a trade off between trapping efficiency and allowed pressure drop.

Case	ΔP	% increase
4.0	102.4	-
4.1	137.3	34.1
4.2	160.4	56.6
4.3	192.7	88.1

Table 12: Obtained pressure from simulations, % column is the increase in pressure compared to an empty channel.

The trapping efficiency in the geometry with 45° angle reached 7.5 % for 5nm and 3.1% for the 10 nm particles. This angle was further evaluated with DPM simulations with the

Brownian diffusion turned off since the commercial available catalyst had the same angle. The highest particle trapping was achieved for case 4.3 (55° angle), 7.8 % and 3.5% for 5nm and 10 nm respectively.

Without Brownian diffusion all the particles in the considered size range end up on 0.75 to 1% in trapping efficiency. The DPM failed to capture inertial effects for larger particles the current simulation. The larger particles are prone to hit the walls directly since it takes longer for them to respond to flow changes. In figure the velocity vectors show small recirculation zones, which can prove beneficial for distributing of particles on the wall.

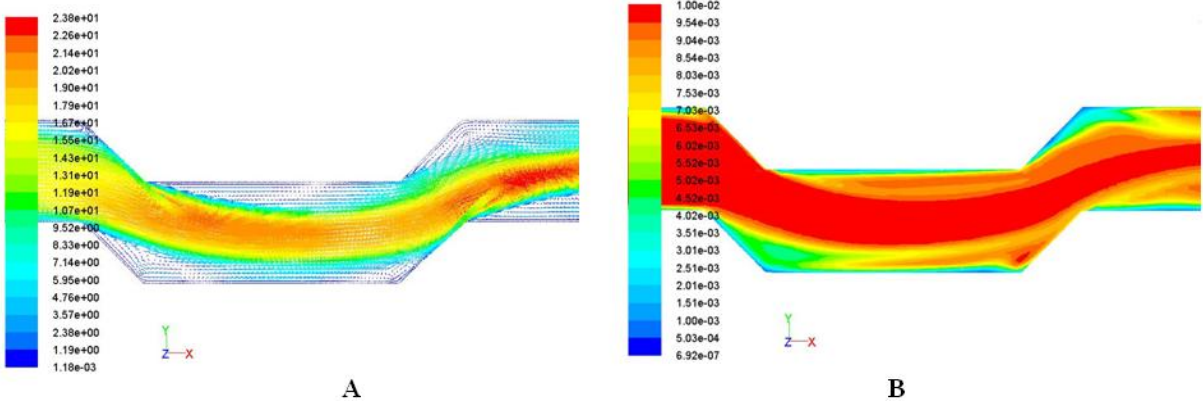


Figure 24: A: Velocity vectors case 4.2. B: Contour of mole fraction for Specie A in case 4.2.

The trapping efficiency for the whole simulation series is given in figure 25 where it is clearly observed that cases with higher angle α and steeper descent of the walls captures more particles directly on the walls.

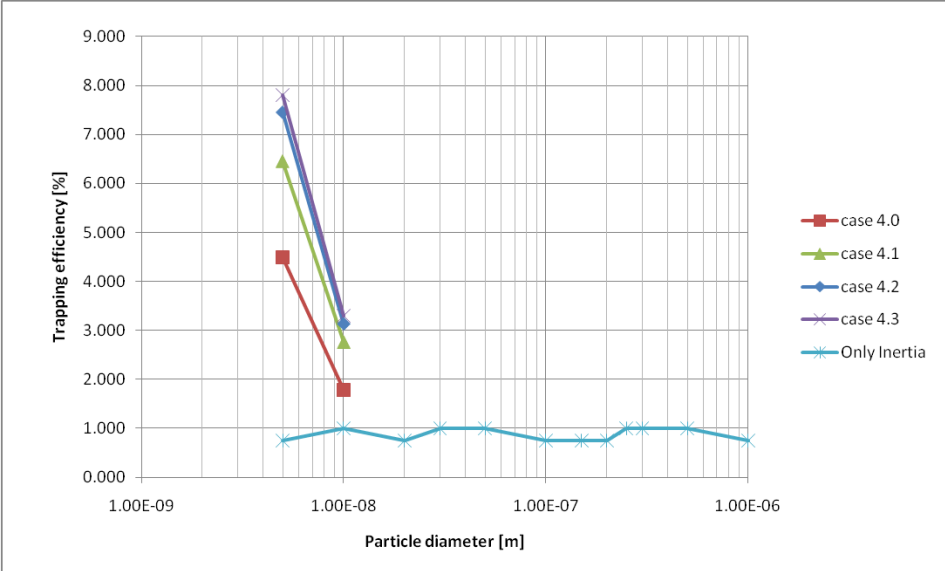


Figure 25: Particle trapping efficiency for 4 different cases with the species method and DPM result for case 4.2 simulation without Brownian diffusion.

4.6 Results for Geometry 5

The use of a single promoter with homogenous porosity and the permeability needed to trap particles to a higher extent than solid promoters was simulated. The simulations setup and result is given in table 13.

case	α	$1/\alpha$	ΔP	%
0	0	0	110.47	-
1	$1 \cdot 10^{-6}$	$1 \cdot 10^6$	110.63	0.14
2	$1 \cdot 10^{-9}$	$1 \cdot 10^9$	153.88	39.3
3	$1 \cdot 10^{-10}$	$1 \cdot 10^{10}$	147.12	33.2
4	$1 \cdot 10^{-11}$	$1 \cdot 10^{11}$	142.7	29.2
5	$1 \cdot 10^{-12}$	$1 \cdot 10^{12}$	142.26	28.8
6	$1 \cdot 10^{-15}$	$1 \cdot 10^{15}$	142.21	28.7

Table 13: study on a porous promoter, pressure drop versus the permeability α and the viscous resistance $1/\alpha$, % = pressure drop increase.

The species trapping efficiency is approximately 5 % for a permeability value of $1 \cdot 10^{-12}$ which is the same value achieved with a solid promoter. This permeability value is also common for commercial wall flow filters for instance a corderite and SIC filter had values corresponding to $0.5 \cdot 10^{-12} \text{ m}^2$ and $1.24 \cdot 10^{-12} \text{ m}^2$ respectively [13]. There are metal foams and other materials available with permeability values as low as $1 \cdot 10^{-6}$.

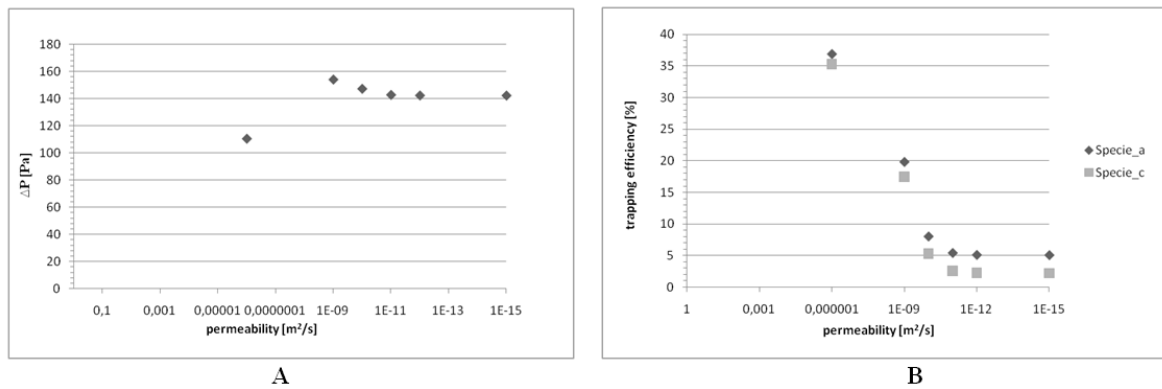


Figure 26: Left: Permeability versus pressure drop. Right: Permeability versus trapping efficiency for specie A and C (representing 5nm and 100 nm particles)

However even if a porous promoter has a high trapping efficiency the rate of the soot oxidation reaction will determine the overall effect of this type of configuration. A low soot oxidation rate would result in a filter cake build up or a clogging of the porous promoter hence the pressure drop increase followed by a decrease in particle trapping efficiency.

4.7 Optimum cases all geometries

To be able to assess the potential advantages with the different monolith catalysts designs, the trapping efficiency for a 5nm particle was plotted versus the pressure drop per meter. Note the length of the catalysts differ so it not possible to compare all of them directly. Nor can interpolated data be used since the trapping efficiency does not scale linearly with length. G4 and G3 can be compared with each other while the remaining is close enough in length to be comparable.

A wall flow filter was added with trapping efficiency of 95% and a pressure drop of 65 000 Pa/m assumed. Note that this is a rough estimation since for a wall flow filter the pressure drop is altered with time and amount of soot deposited. All trapping efficiency data is based on results from the species method since that is most accurate for 5 nm particles.

Geometry 3 with the planes covering the monolith had the highest pressure drop and particles trapping efficiency of all simulated geometries. Even if the pressure drop is high compared to

the other geometries it still less than half of the level reached for the conventional wall flow filter.

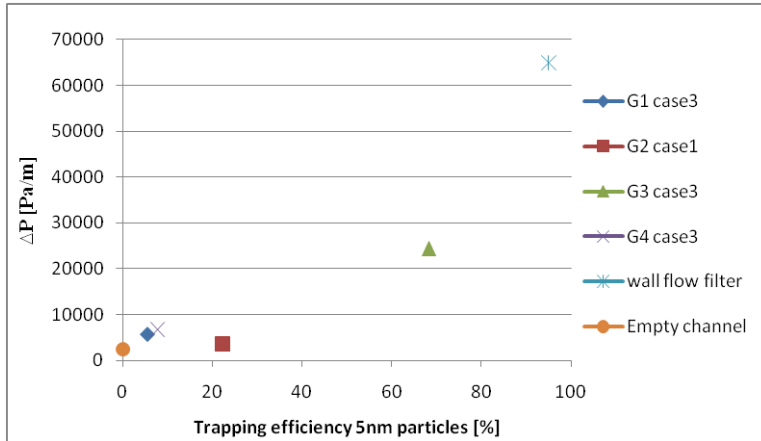


Figure 27: Trapping efficiency of 5 nm particles for the optimal geometries. The catalyst length assumed is 150 mm and the pressure drop is given per length unit. The empty channel correspond to geometry 1 case 0.

4.8 Mass and heat transfer effects

Assuming that the reaction rates are mass transfer limited and that the concentration of pollutant species is zero at the catalyst walls, the conversion can be calculated as

$$X = 1 - \exp\left(-\frac{4ShD_{AB}L}{d_h^2\bar{v}}\right) \quad (4.2)$$

This equation is valid for a square duct monolith and \bar{v} = average channel velocity with a general Sherwood number for the entire channel. (In reality the Sherwood number changes with the development of the velocity profile and assume different values over the promoters).

By taking the conversion of specie A over all the optimal cases for the different geometries a generalized Sherwood number can be calculated from:

$$Sh = -\frac{\ln(1-x)d_h^2\bar{v}}{4D_{AB}L} \quad (4.3)$$

By comparing the different geometries (see figure 28) it can be seen that the geometry 3 (the one with 18 plane inside) has the highest species trapping efficiency for 5 nm particles and Sherwood number of all simulated geometries.

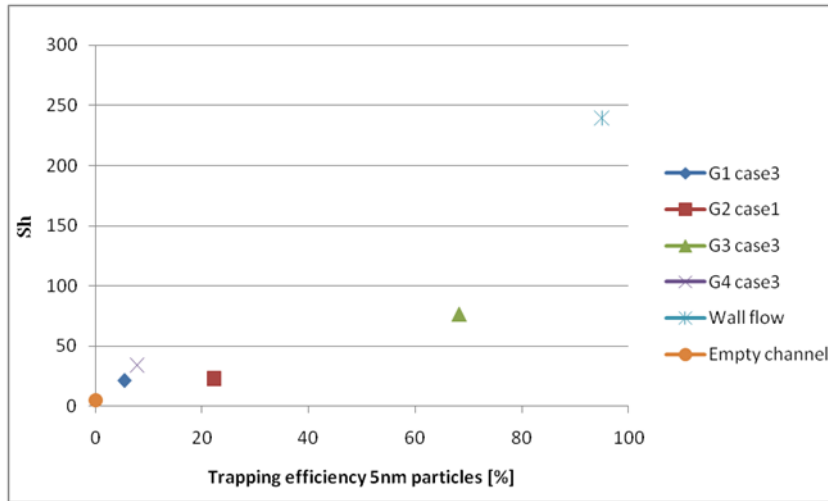


Figure 28: Sherwood number for the optimal geometries of different lengths versus trapping efficiency for 5nm particles. The empty channel correspond to geometry 1 case 0 (length 30 mm).

At laminar flow where the Sc number is equal to the Pr number for gases it is possible to assume an analogy between heat and mass transfer, the Sherwood number is then equal to the Nusselt number. The potential increase in mass transfer then also holds for heat transfer.

5 Conclusions

The result of the discrete phase model is dependent on the injection routine used, distances from walls and between particles and on the number of particles injected. At the same time it is the only method to attain information of inertial effects and to model different forces causing particle deposition and is not limited to a certain particle size. The results provide support for using the species method for quick screening of catalysts designs. Despite from the fact the method is restricted to smaller particles (5 and 10 nm particles) with a prominent Brownian diffusion, it provides better accuracy and shorter simulations times than the DPM method. Particles of smaller size, 1-10 nm were trapped to a larger extent than other considered, with modified monolith catalysts. However trapping 100-1000 nm proved to be more difficult and no increase in deposition of larger particles due to inertial effects were observed.

Data on angular velocities in vortices from the simulated designs clearly show that creating strong enough vortices with promoters for particles to deposit on the walls is difficult. Improving the fluid element mixing with more turbulence would also have to be weighed against the increase in exhaust back pressure. The principle of forcing the flow and particles near walls for instance through the use of planes in a channel, is rather the main option to consider. The comparison of the different designs with a wall flow filter does show that the options for altering a design of a flow through filter, without imposing a too large pressure drop penalty are good.

5.1 Further work

Angles and distances between the promoters used in this thesis can be further optimized, some other aspects to consider is to:

- Investigate if porous promoter is a good option or if the soot accumulation merely clogs the filter faster than regeneration can occur. The most common soot oxidation reactions can then be considered.
- Test porous wall on the flow through filters.
- Asses the benefits of geometries with hole structures interlinking several channel (see figure 5).
- Determine how particle deposition varies with the strength of the vortices created and the linear velocity.
- Since the accuracy of assuming laminar flow inside a flow through monolith is sometimes questioned in the literature, a large eddy simulation for further verification on the results should be performed.

References

- [1] Diesel Exhaust: Critical Analysis of Emissions, Exposure, and Health Effects, Health Effects Institute, 1995-01-01.
- [2] Health Aspects of Air Pollution with Particulate Matter, Ozone and Nitrogen Dioxide Report on a WHO Working Group, Bonn, Germany, 13–15 January 2003.
- [3] A. Clarke, M.C. Law and C. P. Garner, A diesel particulate filter regeneration model with a multi-step chemical reaction scheme, Proc. IMechE. Vol. 219 Part D: J. Automobile Engineering.
- [4] H. Ström, Eulerian-Lagrangian modeling of particle motion in exhaust gas aftertreatment systems, Chalmers University of Technology, 2009.
- [5] J. E. Johnson, D. B. Kittelson, Deposition, diffusion and adsorption in the diesel oxidation catalyst, Applied Catalysis B: Environmental 10 (1996) 117-137.
- [6] R. E. Hayes, S.T. Kolaczowski, Introduction to catalytic combustion, Gordon & Breach, New York, 1997.
- [7] M.Votsmeier, T. Kreuzer, J. Gieshioff, G. Lepperhoff, Automobile Exhaust Control, Ullmann's Encyclopedia of Industrial Chemistry, <<http://mrw.interscience.wiley.com>>
- [8] W. A. Majewski, Diesel Particulate Matter, www.diesel.net, 2010-01-22.
- [9] Källa <http://www.dieselnet.com/standards/eu/hd.php>.
- [10] A.M. Hochhauser, Gasoline and Other Motor Fuels, Kirk-Othmer Encyclopedia of Chemical Technology. 2010-01-20, <<http://www3.interscience.wiley.com>>
- [11] M. Zhen, S. Banerjee, Diesel oxidation catalyst and particulate filter modelling in active Flow configurations, Applied Thermal Engineering 29 (2009) 3021–3035.
- [12] J.Uchisawa, A. Obuchi, A. Ohi, T. Nanba, N. Nakayama, Activity of catalysts supported on heat-resistant ceramic cloth for diesel soot oxidation, Powder Technology 180 (2008) 39–44.
- [13] W. A. Majewski, Diesel Oxidation Catalyst, www.dieselnet.com. 2009-10-20.
- [14] Schaefer-Sindlingera, I. Lappasa, C.D. Vogta, et al, Efficient material design for diesel particulate filters, Topics in Catalysis Vols. 42–43, May 2007.
- [15] L. Andreassi, S. Cordiner, V. Mulone, M. Presti, A mixed numerical-experimental analysis procedure for non blocking metal supported soot trap design. SAE 2002-01-2782),2002.
- [16] W. A. Majewski, Flow-Through Filters, www.dieselnet.com, 2009-10-21.

- [17] A.M. Holmgen, Enhanced Mass Transfer in Monolith Catalysts with bumps on the channel walls, *Ind. Eng. Chem. Res.* 1999, 38, 2091-2097.
- [18] N.H. Schöön, S.L. Andersson, Methods to increase the efficiency of a Metallic Monolithic Catalyst, *Ind.Eng.Chem.Res.*,1993, 32(6), 1081.
- [19] R. Brück, P. Hirth, M. Reizig, Metal Supported Flow-Through Particulate Trap; a Non-Blocking Solution, SAE 2001-01-1950, 2001.
- [20] A. Reck, F.W. Kaiser, F. Jayat, New generation of metallic substrates for catalytic converters in small engine application, SAE 2007-32-0057, 2007.
- [21] K.V.R. Babu,C. Dias, S. Waje, PM Metalit - A Continuously Regenerating Partial Flow Particulate Filter - Concept and Experience with Korean Retrofit Programme, SAE 2008-28-0008, 2008.
- [22] K. W. Aniolek, A CFD study of diesel substrates channels with differing wall Geometries SAE 2004-01-0152, 2004.
- [23] B. Andersson, F. Ekström, Pressure Drop of Monolithic Catalytic Converters Experiments and Modeling, 2002-01-1010.
- [24] C. Crowe, M. Sommerfield, Y. Tsuji, Multiphase Flows with droplets and particles, CRC Press,1998.
- [25] M. Sommerfield, B.Wan Wachem, R. Oliemans, (eds), Best Practice Guidelines for Computational Fluid Dynamics of Dispersed Multiphase Flows (ERCOFTAC /SIAMUF, Göteborg, 2008).
- [26] B. Andersson, R. Andersson, L. Håkansson, et al, Computational Fluid Dynamics for Chemical Engineers, fifth edition , Gothenburg, 2009
- [27] A. Li and G. Ahmadi, Dispersion and Deposition of Spherical Particles from Point sources in a Turbulent Channel Flow. *Aerosol Science and Technology*, 16:209-226, 1992.
- [28] P.J. Mason, B.R Morton, Trailing vortices in the wake of surface-mounted obstacles, *journal of fluid mechanics*, (1987),vol.175, pp 247-293.
- [29] Ansys Fluent 12.0, Users guide

Appendix

A1 The effect of Brownian diffusion on geometry 3

A2 Injection routines

A3 Derivation of a generalized Sherwood number

A3.1 Dimensionless numbers

A4 Geometry 1

A5 Geometry 2

A6 Geometry 4

A7 Geometry 5

A1 The effect of Brownian diffusion on geometry 3

Estimation of the diffusion distance covered by a 150 nm particle at 400°C:

$$D = \frac{k_B T C_c}{2\pi\mu d_p} = 1.33 \cdot 10^{-9}$$

The root square displacement is:

$$\Delta x = \sqrt{2Dt}$$

Assuming a laminar velocity profile above the plate the flow velocity at a distance Δx from the plate is:

$$v = v_{\max} \left(1 - \left(\frac{\Delta x}{h} \right)^2 \right)$$

The shortest retention time for fluid elements on the plate can then be estimated from

$$t = \frac{L}{v}$$

The following expression was derived:

$$\Delta x = \sqrt{2Dt} = \sqrt{\frac{2DL}{v}} = \sqrt{\frac{2DL}{v_{\max} \left(1 - \left(\frac{\Delta x}{h} \right)^2 \right)}}$$

And the length required will be:

$$L = \Delta x^2 \frac{v_{\max} \left(1 - \left(\frac{\Delta x}{h} \right)^2 \right)}{2D}$$

Additionally if the plane is placed so that $h = 1/4$ mm and $v_{\max} = 20$ m/s the following plots can be constructed.

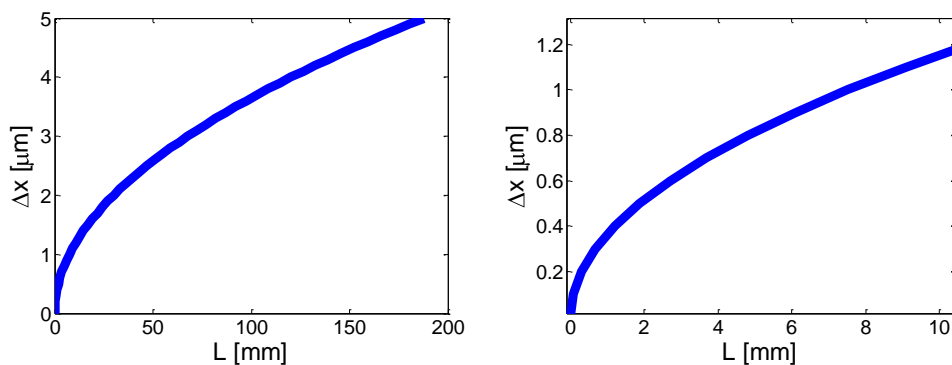


Figure A1: The root square displacement for a 150 nm particle at different lengths.

A 2 Injection routines used

1. Particles injected in all of the equally sized cells over the inlet, referred to as surface routine.
2. The inlet was divided into 20 x 20 intervals for injection of particles, 1/10 mm between each point and the same distance to the wall.
3. In table the result is given for simulations with another injection routine, 5400 particles of the size 5 nm where injected at an interval of 30x30 points with 1/15 mm between each.

A3 Derivation of a generalized Sherwood number

The conversion in a square duct monolith is defined as the inlet concentration minus the outlet concentration:

$$X = \frac{C_{A,in} - C_{A,out}}{C_{A,in}} = 1 - \frac{C_{A,out}}{C_{A,in}}$$

And the flux in mol/m²s:

$$N_{A,in} = k_c(C_A - C_{A,w}) = k_c C_A$$

Where the concentration at the wall is zero ($C_{A,w} = 0$).

The first step in this case is to perform mole balance on species A over a differential element of width dx.

The general mole flux equation:

$$N_{A,in} - N_{A,r} = N_{A,out}$$

$$\bar{v}d_h^2 C_A|_x - k_c C_A|_x^{4dh\Delta x} = \bar{v}d_h^2 C_A|_{x+\Delta x}$$

Dividing by the hydraulic diameter, d_h gives:

$$\frac{dC_A}{dx} = - \frac{4k_c C_A}{d_h \bar{v}}$$

Since $k_c = \frac{ShD_{AB}}{d_h}$ the expression can be rewritten to:

$$\frac{dC_A}{dx} = - \frac{4ShD_{AB}C_A}{d_h^2 \bar{v}}$$

Integration over concentration and channel length gives.

$$\ln \frac{C_{A,out}}{C_{A,in}} = - \frac{4ShD_{AB}L}{d_h^2 \bar{v}}$$

$$C_{A,out} = C_{A,in} \exp \left(-\frac{4ShD_{AB}L}{d_h^2 \bar{v}} \right)$$

Finally an expression for conversion is obtained which contains the Sh.

$$X = 1 - \exp \left(-\frac{4ShD_{AB}L}{d_h^2 \bar{v}} \right)$$

A 3.1 Dimensionless numbers

$$Sh = \frac{k_c d_p}{D_{AB}}$$

$$Sc = \frac{\nu}{D_{AB}}$$

$$Pr = \frac{\nu}{\alpha}$$

$$Nu = \frac{h d_p}{k_g}$$

$$Re = \frac{\rho v L}{\mu}$$

A4: Geometry 1

dp	Inlet	Wall	Outlet	% trapped DPM case 3	% trapped case 0	% trapped species case 3	% trapped case 0
5 nm	334	162	1504	9,72	5,65	5.45	5.45
10 nm		160	1840	8,00	1,80	2.23	2.23
20 nm		156	1844	7,80	0,15	-	-
30 nm		145	1855	7,25	0,00	-	-
50 nm		136	1864	6,80	0,00	-	-
100 nm		135	1865	6,75	0,00	0	0
150 nm		137	1863	6,85	0,00	0	0
200 nm		139	1861	6,95	0,00	-	-
250 nm		139	1861	6,95	0,00	0	0
300 nm		139	1861	6,95	0,00	-	-
500 nm		140	1860	7,00	0,00	0	0
1000 nm		146	1854	7,30	0,00	0	0
Total nr	334	1734	21932	=24000			

Table A4: Euler Lagrange simulation with Fluents discrete phase model (DPM) on case 3, 24000 particles injected in the inlet, species method – represents not simulated, case0 corresponds to an empty channel.

A5: Geometry 2

dp	inlet	wall	Outlet	%
5 nm	0	849	4551	15.72
Total nr:	0	849	4551	5400

Table A5.1: Particle trapping with DPM and injection routine 2 case 1.

Dp	Wall	Outlet	% trapped
5 nm	95	1905	4.75
10 nm	100	1900	5.00
20 nm	100	1900	5.00
30 nm	100	1900	5.00
50 nm	90	1910	4.50
100 nm	85	1915	4.25
150 nm	95	1905	4.75
200 nm	99	1901	4.95
250 nm	110	1890	5.50
300 nm	90	1910	4.50
500 nm	85	1915	4.25
1000 nm	100	1900	5.00
Total nr	1149	22851	=24000

Table A5.2: Results case 2.1 with DPM, Brownian diffusion turned off.

v=10 m/s	Pin	Pout	ΔP	%
Case 2.0	101641	101325	316.36	-
Case 2.1	101796	101325	470.66	48.77
Case 2.2	101796	101325	471.09	48.91
Case 2.3	101798	101325	472.98	49.51
v=5 m/s				
Case 2.0	101472	101325	146.91	-
Case 2.1	101522	101325	196.95	34.06
Case 2.2	101522	101325	197.01	34.10
Case 2.3	101522	101325	197.39	34.36
v =15 m/s				
Case 2.0	101833	101325	507.77	-
Case 2.1	102141	101325	816.27	60.76
Case 2.2	102141	101325	816.07	60.72
Case 2.3	102145	101325	819.82	61.45

Table A5.3: Results all cases with species method.

A6: Geometry 4

dp	Wall	Outlet	% trapped
5 nm	15	1985	0.75
10 nm	20	1980	1
20 nm	15	1985	0.75
30 nm	20	1980	1
50 nm	20	1980	1
100 nm	15	1985	0.75
150 nm	15	1985	0.75
200 nm	15	1985	0.75
250 nm	20	1980	1
300 nm	20	1980	1
500 nm	20	1980	1
1000 nm	15	1985	0.75
Total nr	210	23790	24000

Table A6.1: Case 4.2 DPM simulation run without Brownian diffusion.

Case	Pin	Pout	ΔP	% increase	E (%) 5nm	E (%) 10nm
4.0	101427.4	101325	102.4	-	4.491	1.784
4.1	101462.3	101325	137.3	34.1	6.449	2.762
4.2	101485.4	101325	160.4	56.6	7.459	3.128
4.3	101517.7	101325	192.7	88.1	7.804	3.295

Table A6.2: Species method results for series 4 and pressure drop.

A7: Geometry 5

Case	α	$1/\alpha$	Pin	Pout	ΔP	%
0	0	0	101435.5	101325	110.47	-
1	$1 \cdot 10^{-6}$	$1 \cdot 10^6$	101435.6	101325	110.63	0.14
2	$1 \cdot 10^{-9}$	$1 \cdot 10^9$	101478.9	101325	153.88	39.3
3	$1 \cdot 10^{-10}$	$1 \cdot 10^{10}$	101472.1	101325	147.12	33.2
4	$1 \cdot 10^{-11}$	$1 \cdot 10^{11}$	101467.7	101325	142.7	29.2
5	$1 \cdot 10^{-12}$	$1 \cdot 10^{12}$	101467.3	101325	142.26	28.8
6	$1 \cdot 10^{-6}$	$1 \cdot 10^{15}$	101467.2	101325	142.21	28.7

Table A6.3: Study on a porous promoter, pressure drop versus the permeability α and the viscous resistance $1/\alpha$